Heliyon 5 (2019) e01667

Contents lists available at ScienceDirect

Heliyon

journal homepage: www.heliyon.com

Identification of the iduronate-2-sulfatase proteome in wild-type mouse brain

Carolina Cardona [a,*], Eliana Benincore [a], Natalia Pimentel [a], Luis H. Reyes [a,b], Camilo Patarroyo [a], Alexander Rodríguez-López [a,c], M. Martin-Rufian [d], Luis Alejandro Barrera [a,e], Carlos J. Alméciga-Díaz [a,**]

[a] Institute for the Study of Inborn Errors of Metabolism, School of Sciences, Pontificia Universidad Javeriana, Bogotá, Colombia
[b] Process and Product Design Group (GDPP), Department of Chemical Engineering, Universidad de los Andes, Bogotá, Colombia
[c] Chemistry Department, School of Sciences, Pontificia Universidad Javeriana, Bogotá, Colombia
[d] Central Services Research Support, Proteomics Unit, Universidad de Malaga, Spain
[e] Clínica de Errores Innatos del Metabolismo, Hospital Universitario San Ignacio, Bogotá, Colombia

ARTICLE INFO

Keywords:
Biochemistry
Bioinformatics
Biotechnology
Cell biology
Computational biology

ABSTRACT

Iduronate-2-sulfatase (IDS) is a lysosomal enzyme involved in the metabolism of the glycosaminoglycans heparan (HS) and dermatan (DS) sulfate. Mutations on IDS gene produce mucopolysaccharidosis II (MPS II), characterized by the lysosomal accumulation of HS and DS, leading to severe damage of the central nervous system (CNS) and other tissues. In this study, we used a neurochemistry and proteomic approaches to identify the brain distribution of IDS and its interacting proteins on wild-type mouse brain. IDS immunoreactivity showed a robust staining throughout the entire brain, suggesting an intracellular reactivity in nerve cells and astrocytes. By using affinity purification and mass spectrometry we identified 187 putative IDS partners-proteins, mainly hydrolases, cytoskeletal proteins, transporters, transferases, oxidoreductases, nucleic acid binding proteins, membrane traffic proteins, chaperons and enzyme modulators, among others. The interactions with some of these proteins were predicted by using bioinformatics tools and confirmed by co-immunoprecipitation analysis and Blue Native PAGE. In addition, we identified cytosolic IDS-complexes containing proteins from predicted highly connected nodes (hubs), with molecular functions including catalytic activity, redox balance, binding, transport, receptor activity and structural molecule activity. The proteins identified in this study would provide new insights about IDS physiological role into the CNS and its potential role in the brain-specific protein networks.

1. Introduction

Mucopolysaccharidosis II (MPS II, Hunter syndrome, OMIM 309900) is an X-linked genetic and multisystemic disorder produced by the deficiency of the lysosomal enzyme iduronate-2-sulfatase (IDS, 3.1.6.13). This deficiency leads to the lysosomal accumulation of the glycosaminoglycans (GAGs) heparan (HS) and dermatan sulfate (DS) [1]. MPS II is a progressive disorder with mild to severe clinical manifestations, based on the presence of neurological involvement and age of onset [2]. Patients with severe phenotype are characterized by coarse facial features, short stature, skeletal deformities, joint stiffness, retinal degeneration, chronic diarrhea, progressive hearing impairment, communicating hydrocephalus, and central nervous system (CNS) involvement, with progressive cognitive degeneration [2]. On the other hand, patients with the mild phenotype do not show CNS involvement, but shares similar systemic features to those of the severe phenotype with a reduced rate of progression [1].

Neuropathologically, MPS II patients develop neuronal swelling, dilatation of perivascular space, mild gliosis in the white matter and/or hydrocephalus [3]. Although the molecular mechanism of the neurological dysfunction in MPS II patients is unclear, it is well known that GAGs accumulation leads to secondary accumulation of other macromolecules, organelles and cellular dysfunction, alterations of cellular morphology, impaired autophagy, oxidative stress and neuroinflammatory processes [4, 5]. The therapeutic effects of current enzyme replacement therapy (ERT) for MPS II include improvements in joint

* Corresponding author.
** Corresponding author.
E-mail addresses: carolina.ramirez.cardona@gmail.com (C. Cardona), cjalmeciga@javeriana.edu.co (C.J. Alméciga-Díaz).

https://doi.org/10.1016/j.heliyon.2019.e01667
Received 30 January 2019; Received in revised form 30 March 2019; Accepted 2 May 2019

mobility, gait, pulmonary and respiratory functions, reductions in liver and spleen size and urinary GAGs excretion [6, 7, 8]. However, the CNS damage persists, since the enzyme used in the current ERT cannot cross the blood-brain barrier (BBB) [9].

At present, a specific brain-interactome of IDS has not been described. The study of protein-protein interaction (PPI) networks facilitates the identification of new biomarkers and the identification of new therapeutic targets. Recent advances in several fields have contributed to the study of pathological mechanisms of neurodegenerative disorders using neurochemistry and omics approaches [10, 11]. In this study, we applied immunohistochemical and proteomics methodologies to shed light on the IDS distribution in mouse brain under physiological conditions and get insights into the physiological role of IDS in the mouse brain. The IDS-proteome identification was carried out via affinity chromatography and analysis of IDS-native protein complexes from wild-type mouse brain through Blue Native Page (BN-PAGE). One hundred and eighty-seven putative IDS partner proteins were identified, from which 31 were predicted as highly connected nodes (hubs). Functional classification analysis revealed that most of the proteins were identified as hydrolases, cytoskeletal proteins, transporters, transferases, oxidoreductases, nucleic acid binding proteins and enzyme modulators, among others. Seventeen proteins were predicted to have a direct interaction with IDS, which were functionally classified with GO terms mainly involved in axogenesis, exocytosis, vesicle-mediated transport, and neuron projection development. The interaction of IDS with fructose-bisphosphate aldolase C (ALDOC), 14-3-3 protein gamma, 14-3-3 protein zeta and myelin proteolipid protein (PLP), was confirmed by immunoprecipitation. In addition, the comparative analysis of high-molecular mass complexes (HMC) and low-molecular mass complexes (LMC) permitted the prediction of hubs with molecular functions including axogenesis and cell migration (DnyC1h1), redox protection (Prdx1, Prdx2 and TXN1), immuneresponse activity (TNPI2) and glycolytic activity (Atp5b and ENO1). The proteins identified in this study provide relevant information about different physiological roles for IDS and could be promising candidates for further functional validations.

2. Materials and methods

2.1. Purification and characterization of IgYs anti-IDS for immunodetection

Antibody purification. To identify the regional distribution and subcellular presence of IDS in mouse brain, IgY anti-$IDS_{99\text{-}122}$ (anti-peptide against amino acids 99–122) and anti-$IDS_{262\text{-}286}$ (anti-peptide against amino acids 262–286), previously produced [12], were purified with a thiophilic resin under standard protocols [12]. After the thiophilic purification, 4 mL of each group of immunoglobulins solution (anti--$IDS_{99\text{-}122}$ and $IDS_{262\text{-}286}$) were mixed with 0.1 volume of Tris-HCl 1M, pH 8.0, then ammonium sulfate was added at 15 min intervals until reaching a 50% of saturated solution (29.5 g/100 mL) and keeping with gentle agitation during 1 h at 4 °C. The immunoglobulins solution was centrifuged at 10,000g during 20 min, resuspended in 0.5 volumes of Tris-HCl 10 mM, pH 7.5, and dialyzed overnight in the same buffer. Two mL of each isolated IgY fractions (anti-$IDS_{99\text{-}122}$ and $IDS_{262\text{-}286}$) were diluted 10-fold with Tris-HCl 10 mM, pH 7.5, and slowly passed through an IDS-column (0.5 mL min^{-1}) (See **Chromatography columns construction**). The same column was used to purify these two anti-peptides. The column was washed two times with 10 mL of Tris-HCl 10 mM, pH 7.5, and two times with Tris-HCl 10 mM, 0.5 M NaCl, pH 7.5. The acid-sensitive IgY fractions were eluted with 5 mL of 100 mM glycine pH 2.5 and collected in a tube containing 1 mL of 1 M Tris-HCl, pH 8.0. The column was washed with 10 mM Tris-HCl, pH 8.8, and the base-sensitive IgY fraction was then eluted with 5 mL of 100 mM triethylamine pH 11.5, on a tube containing 1 mL of 1 M Tris-HCl pH 8. Base and acid-sensitive fractions were pooled, dialyzed against PBS 1X (4.3 mM Na_2HPO_4, 137 mM NaCl, 2.7 mM KCl, 1.4 mM KH_2PO_4, pH 7.4) and concentrated approximately 6-fold using 10 kDa Amicon® Ultra Centrifugal filter (Millipore). The aliquots were stored with 0.02% sodium azide at -20°C.

SDS–PAGE and Western blotting. The specificity of the chicken anti-IDS antibodies used in this study was previously demonstrated [12]. Nevertheless, before the evaluation of the IDS distribution in wild-type mouse brain, the cross-reactivity of the two antibodies was assayed in brain and liver protein extracts. For this purpose, SDS–PAGE was performed as described by Laemmli *et al.* [13]. We immunoblotted the brain and liver proteins from mouse homogenates, human erythrocytes and human recombinant IDS-like protein expressed in *E. coli* K12 [14].

Equivalent volumes of purified recombinant proteins and total protein extracts from liver and mouse brain (30 ng–40 μg of total protein respectively) were loaded and ran on 12 % sodium dodecyl sulfate-polyacrylamide gels electrophoresis (SDS-PAGE) and electroblotted onto nitrocellulose membranes (GE Healthcare Life Science). Membranes were blocked with a blocking buffer containing PBS 1X, 0.3% Tween 20, and 5% Bovine serum albumin (BSA, Sigma-Aldrich) at RT for 1 h. After blocking, the membranes were incubated overnight at 4 °C with anti-IDS antibodies: anti-$IDS_{99\text{-}122}$ and anti-$IDS_{262\text{-}286}$, at 1:500 dilutions in blocking buffer. A peroxidase conjugated goat anti-chicken (Promega, Wisconsin) was added (1:2000) for 1 h at room temperature (RT). The specific protein bands were visualized using the enhanced chemiluminescence technique (SuperSignalTM West Pico Chemiluminescent Substrate, Thermo Fisher Scientific). The molecular masses were determined by using Precision Plus Protein™ (BioRad), including five reference bands (14, 25, 45, 66 and 116 kDa). The tissue specificity analyses showed that the anti-$IDS_{262\text{-}286}$ exhibited the highest specificity in brain and liver, detecting the expected bands, then it was selected to be used in the rest of this work (Fig. 1).

Brain tissue extraction. Adult male C57BL/6 mice (12 weeks old; n = 12) were obtained from the Comparative Biology Unit at Pontificia Universidad Javeriana under approved protocols of the Institutional Animal Care and Use Committee. For immunohistochemical studies, mice (n = 3) were deeply anesthetized and transcardially perfused with ice-cold fixing solution (4% paraformaldehyde, 75 mM lysine, and 10 mM sodium metaperiodate). After overnight post-fixation in fixing solution, the brains were cryoprotected (30% sacarose) and sectioned (3 μm) in a vibrotome. The brain of a single animal was used for each replica and at least three independent experiments were performed in each experimental purpose.

Immunohistochemistry and immunofluorescence detection of

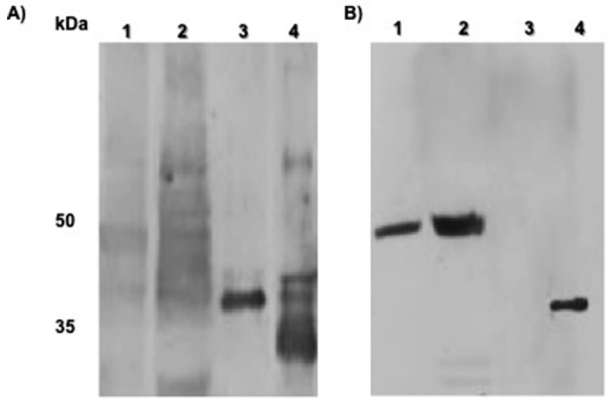

Fig. 1. Western blotting analysis. Cross-reactivity assessment for chicken polyclonal antibody. A) Anti-$IDS_{99\text{-}122}$ (anti-peptide against amino acids 99–122). B) Anti-$IDS_{262\text{-}286}$ (anti-peptide against amino acids 262–286). Equivalent amounts of protein extracts (35 μg) of whole tissue extracts liver (lane 1), brain (lane 2), leukocytes (lane 3) and 10 μg of non-purified IDS recombinant protein (lane 4) were loaded and run on 10 % sodium dodecyl sulfate-polyacrylamide gels electrophoresis (SDS-PAGE) and electroblotted onto nitrocellulose membranes (the unedited version is provided in Supplementary Images).

native IDS. Free floating sections were incubated with 50 mM citrate, pH 6.0, during 30 min at 80 °C followed by 30, 15 and 15 min of endogenous peroxidase, biotin, and avidin inactivation, respectively (Blocking Kit, Vector Labs, United Kingdom). Avidin/biotin inactivation was used just for immunohistochemistry detection. The sections were blocked with blocking buffer (PBS 1X, 0.2% Triton X-100, and 5% BSA). After blocking, sections were incubated with primary antibodies against glial fibrillary acidic protein (GFAP) (1:000, Abcam, Cambridge, MA, USA) during 24 h, overnight at 4 °C. Finally, the sections were incubated with anti-$IDS_{262\text{-}286}$ (1:250) for 24 h at RT. All immunohistochemical studies were tested using negative controls (omitting the primary antisera) and no immunoreaction products were detected in any case.

For immunohistochemistry, the tissue-bound primary anti-IDS antibody was detected by incubating with biotinylated anti-chicken IgG (Vector Labs) for 1 h at RT (1:500 dilution) and then with extravidin-peroxidase conjugate (Sigma-Aldrich) for 1 h at RT (1:2,000 dilution). Immunoreaction was visualized with 0.05% 3-3′-diaminobenzidine tetrahydrochloride (Sigma-Aldrich), 0.03% nickel ammonium sulphate, and 0.01% H_2O_2 in PBS 1X. Sections were mounted onto collagen-coated slides, dehydrated in graded ethanol, cleared in xylene and coverslipped with DPX mounting medium (Sigma-Aldrich). To identify cell morphology, hematoxylin and eosin staining (H&E) was performed after immunohistochemistry according to a standard procedure [15].

For double immunofluorescence labeling of GFAP/IDS, primary antibodies were detected by the corresponding Alexa 568/488 secondary antibodies (1:1,000 dilution, Thermo Fisher Scientific). Sections were then mounted onto collagen-coated slides, and coverslipped with PBS 1X containing 50% glycerol and examined under a confocal laser microscope (Olympus FLUOVIEW FV1000).

2.2. IDS-proteome isolation and characterization

Heterologous expression of recombinant IDS in *Pichia pastoris* GS115. The production of human recombinant IDS (rhIDS) in the yeast *P. pastoris* GS115 was carried-out as previously described [16]. Briefly, human IDS cDNA (GenBank accession number NM_000202.6, kindly donated by Dr. Shunji Tomatsu) was inserted in the pPIC9 plasmid (Thermo Fisher Scientific, San Jose, CA, US) downstream of the α-factor secretion signal from *S. cerevisiae* to produce pPIC9-IDS. The expression vector was linearized and used to transform competent cells of *P. pastoris* GS115 (Thermo Fisher Scientific). Bioreactor production of rhIDS was done at 1.65 L scale in a KLF 3.7 L Bioengineering reactor. Cells were cultured in modified fermentation medium FM22 (composition per liter: $KH_2PO_4$25.74 g, $(NH_4)_2SO_4$ 3 g, K_2SO_4 8.58 g, $CaSO_4$ $2H_2O$ 0.6 g, glycerol 40 g, $MgSO_4$ $7H_2O$ 7.02 g, biotin 4×10^{-5}% w/v, supplemented with *Pichia* trace minerals PTM4 1.0 mL). Protein production was done in two phases: *i)* a batch culture with glycerol to achieve 60 g L^{-1} biomass, and *ii)* a fed-batch induction phase with methanol. Cultures were done at 28 °C and pH 5.0 ± 0.2 during 96 h. Culture medium (~1.7 L) was filtered sequentially through Whatman™ paper No. 1 and 42, and 0.45 and 0.22 μm polyether sulphone membranes (Pall Corp, Port Washington, NY, USA). The permeate was ultra-filtered through a 30 kDa cut-off membrane (Millipore, Billerica, MA, USA) up to reach a final volume of 20 mL. Finally, the retentate was diafiltered against 25 mM sodium acetate buffer (pH 5.0 ± 0.2) and concentrated up to 10 mL by using 10 kDa Amicon® Ultra Centrifugal filter (Millipore**).** The rhIDS was purified by using a cation exchange chromatography with a Macro-Prep High S support column (Bio-rad, Hercules, CA, USA) equilibrated with 25 mM potassium acetate, pH 5.0 ± 0.2, and eluted with a linear gradient of 0–0.5 M NaCl. The purified protein was dialyzed in binding buffer ($NaHCO_3$ 200 mM pH 8.3, NaCl 500 mM) and then pooled in 1 mL. Gel filtration chromatography analysis of purified rhIDS was performed on a 16/60 Sephacryl-200 column (1 × 120 mL) with maximum pressure over the packed bed (0.15 MPa, 1.5 bar) during the operation process (GE Healthcare Life Science, Pittsburgh, PA, USA), following a standard procedure. Protein samples from ion exchange and molecular exclusion chromatography were pooled and 15 μL of each fraction was loaded on 12% acrylamide gels and 3% stacking gel for SDS-PAGE, staining with Coomassie Blue R-250 (Sigma-Aldrich) and Western blot analyses.

Chromatography columns construction. To construct pre-clearing columns, 10 mg of BSA (Sigma-Aldrich, St. Louis, MO, USA) were combined with CNBr-activated Sepharose 4B (GE Healthcare Life Science) in coupling buffer (0.5 M NaCl, 0.2 M $NaHCO_3$, pH 8.3). The coupling reaction proceed on a tilting shaker for 2 h at 4 °C, after which the remaining active groups were quenched with 2 column volumes of 1 M ethanolamine (Sigma-Aldrich) for 1 h at RT. After quenching, all columns were washed 3 times with acid (0.1 M sodium acetate, pH 4.0 containing 0.5 M NaCl) and basic buffers (0.1 M Tris-HCl, pH 8.0 containing 0.5 M NaCl) according to the manufacturer's specifications. rhIDS-columns were constructed in a similar manner. Briefly, 10 and 1 mg of rhIDS diluted in coupling buffer were used for coupling to 1 mL and 500 μl of pre-activated and swelled CNBr dry resins, respectively. All columns were previously equilibrated with binding buffer. Column containing 1 mg of recombinant protein was used for antibody purification by affinity chromatography.

Affinity Chromatography. Affinity chromatography is a powerful and comprehensive large-scale method to isolate proteins from complex mixtures based on a reversible interaction between a protein or group of proteins and a specific immobilized ligand [17, 18]. Brain extracts from 3 mice were pre-cleared over 3 BSA columns and then applied to the rhIDS-Sepharose columns (a new column was manufactured for each experiment) with a peristaltic pump. Ten column volumes of wash buffer (20 mM Tris-HCl, pH 8.0, 0.35 M NaCl, 1 mM EDTA and 0.25 M sucrose) were used to wash both BSA and rhIDS-Sepharose columns. The elution was then performed with 5 column volumes of elution buffer (20 mM Tris-HCl, pH 8.0, 1 mM EDTA, 0.25 M sucrose, and 1 M NaCl) and then, 5mL of 100% acetone was added and incubated overnight at -20 °C. The acetone precipitates were centrifuged at 13,000g during 20 min, and the supernatants removed. After air-drying, 25 μL of 2X SDS-PAGE sample buffer were added to evaluate the protein presence by SDS-PAGE and silver staining. Protein bands were excised from the gels and destained with 1:1 solution of 30 mM potassium ferricyanide and 100 mM sodium thiosulfate. The reduction and alkylation were done with 10 mM DTT and 55 mM iodoacetamide respectively. In gel-digestion was done in 13 ng/μL of trypsin (Promega) at 37 °C for 16 h [19], with a Digest Pro (INTAVIS Bioanalytical Instruments**).**

Indirect co-immunoprecipitation protocol. To validate some of the novel rhIDS protein-protein interactions (PPIs) identified, six proteins, highly scored using Mascot probability-based scoring, were selected to be confirmed by co-immunoprecipitation assay. Three of the selected proteins were from the IDS global network; while the other three proteins were from the primary IDS network created with GENEmania. We also selected these proteins based on a high sequence coverage percentage (% SC) and the availability of commercial antibodies tested for immunoprecipitations. For the indirect co-immunoprecipitation, each antibody was first incubated with total brain extract to allow the formation of the antibody-antigen complex in solution. Protein A or G coupled to magnetic beads were then incubated with the pre-formed antibody-antigen complex.

The samples were prepared using 100 μg of mouse brain lysate and 3 μg of each antibody: anti-aldolase C (Abcam, ab87122), anti-Hsc70 (Abcam, ab2788), anti-synaptotagmin (Abcam, ab13259), anti-myelin PLP (Abcam, ab183493), anti-14-3-3 gamma (Abcam, ab155050) and 14-3-3 (Abcam, ab9063). Rabbit IgG isotype control (Sigma-Aldrich, 31235) was used as negative control for non-specific protein background. Samples were incubated for 2 h at 4 °C with continuous mixing, followed by the addition of 50 μL of protein G (Pure proteome™ Protein G Magnetic Beads, Millipore-Sigma), previously washed with 500 μL of PBS 1X containing 0.1% Tween 20. The samples were incubated at RT for 10 min with continuous mixing. Samples were washed and eluted according to the manufacturer's instructions. After elution, samples were separated by SDS-PAGE and transferred to a cellulose membrane. Prior to applying the

BSA blocking and primary antibodies, we performed an IgG blockage (heavy and light chains) with anti-rabbit IgG against whole molecules (Sigma-Aldrich). Immunodetection was performed with anti-$IDS_{262-286}$ (diluted 1:250) and horseradish peroxidase conjugated Anti-Chicken IgY (Promega).

2.3. Native IDS-complexes isolation from cytosolic fractions

Blue Native Polyacrylamide Gel Electrophoresis (BN-PAGE) and immunoblotting. Native protein complexes can be isolated in accordance to their molecular mass via BN-PAGE, charging proteins negatively using Coomassie dye. This methodology offers several advantages like separation under native conditions and identification of subunit composition [20]. We used BN-PAGE to isolate native IDS-complexes from wild-type mice and to evaluate the IDS-protein complexes profiles in brain extracts. As a complementary method, to enrich the samples and to resolve protein complexes, the brain lysates were sub-fractionated and analyzed by BN-PAGE. Three-months old wild-type (C57BL/6) mice males were used in this study. To analyze IDS-protein complexes, approximately 20 mg of brain and liver were homogenized in 5 volumes of homogenization buffer [20 mM Tris pH 7.0, 10% glycerol, 500 mM of alpha-aminocaproic acid, 20 mM NaCl, 2 mM EDTA pH 8,0, Triton X-100 0.5% and 1 mM phenylmethanesulfonyl fluoride (PMSF)]. The homogenates were centrifuged at 3000g, for 10 min at 4 °C and the supernatants (S1) were transferred to a fresh tubes. The cell pellets were resuspended in 3 volumes of homogenization buffer, incubated 30 min and centrifuged at 3,000g during 10 min. The supernatant was mixed with S1 to get the total protein extract. Finally, the samples were dialyzed against the homogenization buffer containing 0.1% Triton X-100. BN-PAGE was performed as previously described [21]. Briefly, a gradient separating gel was prepared (4–15%) and used to perform electrophoresis under native conditions. Cathode buffer, containing 0.02% of Coomassie G250, was added to the upper chamber and 60 μg of samples was loaded. BN-PAGE was performed at 8 °C and power supply was setup at 100 V until the samples entered to the gel. The electrophoresis was continued at 15 mA, 500 V, and 8 °C during 10 h. After the cathode buffer has displaced about one-third of total running distance, the cathode buffer was diluted 10 times for better detection of protein bands and to avoid the interference with protein binding to the nitrocellulose membranes. Proteins were transferred to nitrocellulose membrane at 100 V during 2 h. High molecular weight calibration kit for native electrophoresis (GE Healthcare Life Science) was used to identify molecular masses. The identification of IDS-protein complexes was performed by Western blot using anti--$IDS_{262-286}$ antibody as previously described. On the other hand, cytosolic fractions were obtained with ProteoExtract® Subcellular Proteome Extraction Kit (S-PEK, Millipore-Sigma), according to the manufacturer's instructions.

Antibody removal. For proteins electrobloted via BN-PAGE, once IDS complexes were detected and the proteins of interest were excised according to the western blot signal, the antibody removal was carried out by three washes of PBS 1X for 10 min and three washes with stripping buffer (1.5% glycine, 0.1% SDS, 1% Tween, pH 2.2) for 10 min at RT. Then, 90 μL of acetone per 4 mm^2 of membrane were added, the samples were mixed on a vortex and incubated for 30 min at RT. The samples were centrifuged 10 min at 14,000g, and the supernatants were carefully removed, air-dried and resuspended in PBS 1X for mass spectrometry identification.

Mass Spectrometry. Mass spectrometry sample handling and protein identification were performed at the Unidad de Proteómica (Servicios Centrales de Apoyo a la Investigación, Málaga, España). Tryptic peptides were separated on a nano-HPLC Agilent 1200 system with a ZORBAX 300SB-C18 column (5 × 0.3 mm, x 250 cm, 5μm; 300 Å in pore diameter) using a gradient of 98% H_2O: 2% acetonitrile (ACN)/0.1% formic acid (FA), at flow rate of 20 μL/min, during 6 min. The amaZon speed 3D ETD system (Bruker Daltonics, Billerica, MA) was operated with a Captive-SprayTM nano electrospray source. A full scan range was set at 300–1,500 (*m/z*), followed by an MS spectrum in tandem by a non-destructive inductive charge detector (ICD) of the eight most abundant ions. The ion charge control was set at 200,000, with a maximum accumulation time of 200 ms. The software ProteinScape 3.1 (Bruker Daltonics) equipped with Mascot 3.1 search engine (Matrix Science) was used for protein identification, matching the MS/MS data against the database Swiss-Prot. Dynamic exclusion was set up behind each two spectra during 12 s after fragmentation to avoid the isolation of the same *m/z*. The searching parameters were set as following: carbamidomethylation of cysteines as fixed modification, methionine oxidation as variable modification and up to two missed cleavages were allowed as well. The MS and MS/MS mass tolerances were 0.6 Da and 0.5 Da, respectively. The MS/MS spectra with a score above the threshold defined by Mascot were validated manually.

Bioinformatics analyses. The data sets collected by MS/MS were annotated and summarized according to shared categorical data for gene ontology, protein domain and biochemical pathways with Database for Annotation, Visualization, and Integrated Discovery (DAVID 6,7) [22]. The Protein Analysis Through Evolutionary Relationships (PANTHER, version 11.1) [23] was used for classification analysis in biological processes. The protein networks were created in Cytoscape (version 3.5.1) using the geneMANIA plugin for protein-protein interaction prediction [24]. The detection of protein complexes with their respective confidence values in protein-protein interaction networks was done with ClusterONE [25]. We applied Contextual Hub Analysis Tool (CHAT) to identify hub genes based on their (weighted) connectivity scores. Genes with statistically detectable connectivity (adjusted $p < 0.05$) were defined as hubs [26].

3. Results

IDS distribution in mouse brain. The immunodetection assays were performed with anti-peptide anti-$IDS_{262-286}$, due to the high specificity in brain and the respective controls (Fig. 1). The immunohistochemistry (IHC) analyses were carried out in mouse brain sections after perfusion with 4% paraformaldehyde, 75 mM lysine, and 10 mM sodium metaperiodate (Fig. 2). Immunoreactivity was detected in different regions of the brain in all tested mice (n = 3). The light microscopic examination of cerebral cortex shows six distinguished layers by displaying of cell nuclei stained darkly by H&E staining (Fig. 2A-B), and a strong immunoreactivity for IDS (brown staining) throughout layers I-VI from cerebral cortex. The IDS immunoreactivity was clear in all cortical layers even within the cellular soma from layer III (Fig. 2C), which is composed of medium-sized pyramidal nerve cells [27]. IDS was observed in nerve cells of the same cortex layer in sections exposed only to the anti-IDS antibody (Fig. 2D). It was also observed immunoreactive cells with different morphology (Fig. 2E). Finally, we also distinguished positive reactivity in the different layers of cerebellum (Fig. 2F), even within some cell populations in the molecular layer (Fig. 2F, **boxed image)**.

The results of astrocyte IDS expression obtained in mouse brain tissues were validated by double immunofluorescence labeling with anti IDS antibody and anti-GFAP (astrocyte marker) employing laser scanning confocal microscopy in cerebellum (Fig. 3A-C) and cerebral cortex (Fig. 3D-F).

Brain IDS proteome isolation. We isolated IDS-binding partners using rhIDS expressed in *P. pastoris* GS115. This recombinant protein was used to isolate the IDS-binding partners, since it is expected that it shares a high structural similarity with the wild-type human IDS, due to the similar post-translational modifications carried out by *P. pastoris* [28]. The rhIDS was purified by anion exchange and molecular exclusion chromatography to obtain pure protein for proteome isolation (Fig. 4A). The protein purity was evaluated after each purification step via SDS-PAGE and Western blot (Fig. 4B). The Western blot analysis showed the presence of mature forms for IDS (Fig. 4B) above 75 and 15 kDa, approximately.

Before IDS-proteome isolation, total protein extracts from 3 wild-type

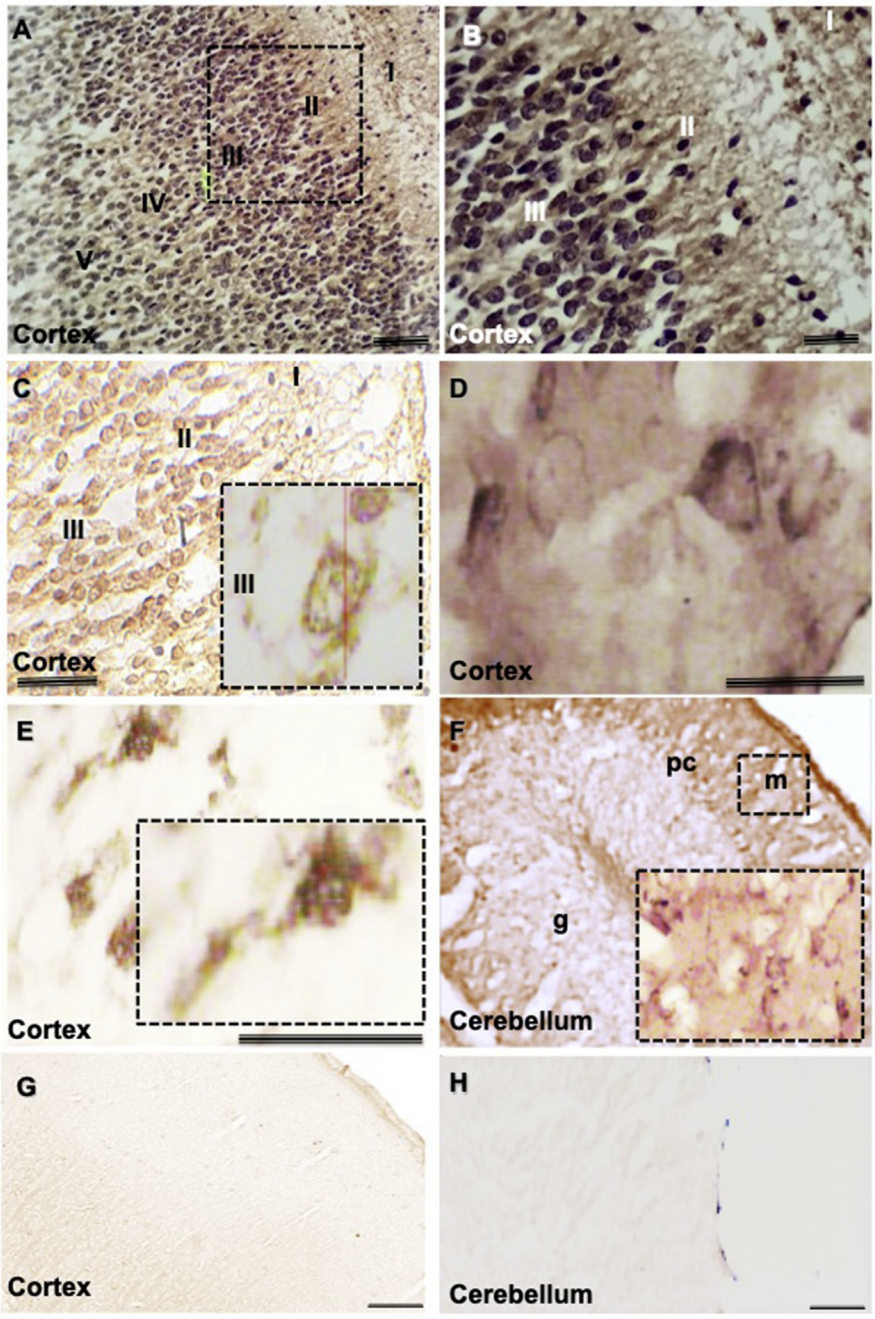

Fig. 2. IDS immunohistochemistry in mouse brain. The immunoreactivity reveals robust staining in cerebellum and cortex (brown staining). A) cortex; B) magnified image indicating the presence of IDS in cerebral cortex layers (amplified image in C and detailed image inset after the H&E removal); D) detail of a positive cellular reactivity in the layer III; E) immunopositive nerve cell with different morphology; F) positive immunoreactivity for cerebellum (magnified image for a nerve cell from the molecular layer); (G and H) negative controls. Scale bar: 200 μm m, molecular layer; P, Purkinje cell layer; g, granular cell layer.

C57Bl/6 adult mice were passed through a BSA-Sepharose column, to capture non-specific binding-proteins [29]. Eluted fractions were used for affinity purification under high stringency conditions to isolate high-affinity proteins. The bound proteins were eluted by increasing the ionic strength with elution buffer, separated by SDS-PAGE and excised after silver staining (Fig. 4C).

Based on Mascot results after nano-HPLC-MS/MS analysis of IDS-proteome, we used the following two criteria to select the proteins for bioinformatic analysis: *i*) proteins must be found in the three independent experiments (full data of each isolated proteome are provided in Supplementary Data), and *ii*) the proteins must have a score above the uncertainty threshold automatically calculated by Mascot Search Engine (individual ions scores >45 indicate identity or extensive homology, p-value <0.05) [30, 31]. We also used the Contaminant Repository for Affinity Purification (CRAPome) to determine the proteins with a higher propensity to be contaminants. A dataset of contaminants was downloaded from the CRAPome database version 1.1 and the proteins observed in two or more CRAPome datasets were considered as contaminants and removed for subsequent analysis (Table 1).

Table 2 lists the 187 proteins that were identified in three independent experiments with their respective ions score in an MS/MS search and the percentage of the protein sequence covered by the identified peptides, after removal of the contaminant proteins identified by CRAPome. The biological dataset was analyzed with geneMANIA at Cytoscape to find functional associations networks between the selected proteins [32]. We performed the analyses considering physical interactions and predicted network category (Fig. 5A). This last category predicts functional relationships between genes and often protein interactions, by mapping known functional relationships from another organisms, using "assigned based on query gene weighting" to increase genes interactions as much as possible among them [24] (Fig. 5A). Noteworthy, we found a primary network for IDS composed of 17

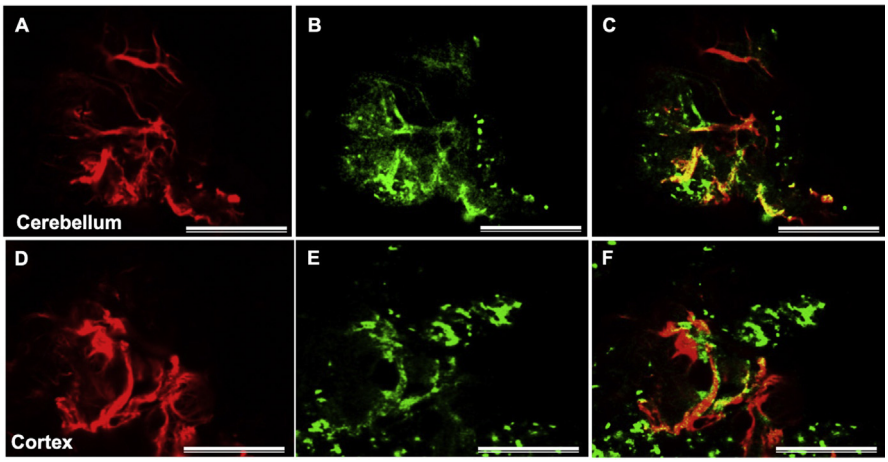

Fig. 3. Confocal microscopy. Double immunofluorescence for GFAP (red) and IDS (green) in cerebellum (A-C) and cortex (D-F). Scale bars: 20μm. The Pearson correlation value for C and I was calculated by Fiji Is Just (Image J) with 1.000 of R-total and 91,13 % of co-localization volume.

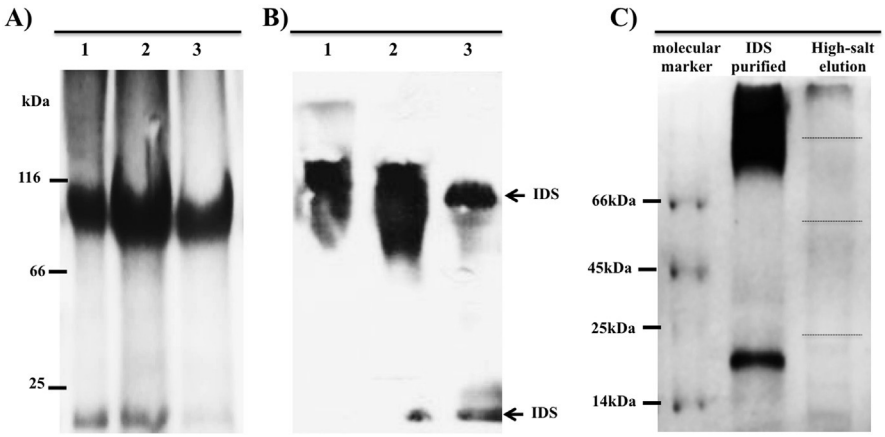

Fig. 4. Purification of recombinant IDS and proteome isolation. A) SDS of size-exclusion chromatography. The collected volumes were at maximum peak height corresponding to the protein IDS. The pooled fractions were analyzed by SDS-PAGE after molecular exclusion chromatography on Sephacryl-200. B) The presence of IDS was confirmed by Western blot using specific antibodies against human IDS and was visualized by chemiluminescence. Lanes 1–3 the collected fractions of the most abundant peak. C) The purity of recombinant protein was evaluated through silver staining before covalent coupling to the sepharose matrix pre-activated with cyanogen bromide. Under reducing conditions, the bands corresponding to the heavy chain (above 75 kDa) and the light chain (above 15 kDa) were observed. The IDS-binding proteins eluted with high astringency were precipitated, loaded for SDS-PAGE and, once stained, lanes were cut in four pieces (highlighted with segmented lines) for MS/MS analysis (the unedited version of this figures are provided in Supplementary Images).

Table 1
Proteins observed in two or more CRAPome datasets.

Uniprot_ ID	Ave_SC	Num_ Expt	CC195	CC196	CC197	CC198	CC199
Alb	16.33	3	36	5	0	8	0
Hnrnpa2b1	7.0	4	0	13	7	3	5
Hnrpu	5.25	4	0	6	4	3	8
Hspa8	7.8	5	5	10	3	2	19
Hspa1l	4.4	5	3	6	3	2	8
Grp78	1.0	1	0	0	0	0	1
Hsc73	4.0	4	2	9	2	0	3
Nefh	8.5	2	0	0	0	9	8
Tuba1a	9.6	5	9	18	6	9	6
Tuba1b	14.0	5	12	26	9	13	10
Tuba1c	13.6	5	11	25	9	13	10
Tuba4a	9.4	5	9	18	7	7	6
Tubb5	15.8	5	18	23	19	10	9
Tubb2a	8.0	5	9	10	10	6	5
Tubb4a	8.0	5	7	4	11	10	8
Tubb4b	10.6	5	11	12	12	10	8
Tubb6	3.8	5	3	1	6	4	5

* The first column corresponds to the protein IDs, the second column lists the averaged spectral counts (Ave_SC) across the experiments in which each protein was identified, and the spectral counts in each selected experiment (CC195-CC199). The Num_Expt is the number of experiments (five experiments selected in the control panel) in which the protein was identified.

proteins primarily involved in processes such as vesicle-mediated transport, exocytosis, neuron projection development and axogenesis by using orthologous protein databases (Fig. 5B). In addition, the 187 identified proteins were classified as hydrolases, cytoskeletal proteins, cell adhesion molecules, oxidoreductases, transferases and transporters among others, via gene ontology using PANTHER (Fig. 6). Finally, 31 highly connected nodes were predicted with CHAT; which include mostly several members of the adapter proteins 14-3-3, heat shock proteins, enzyme modulators, oxidoreductases, transmembrane receptors and glycolytic enzymes (Table 3).

Co-immunoprecipitation of IDS-binding partners. The processed form of IDS (42 kDa approximately) was detected in four immunoprecipitation reactions. Although the contamination by anti-IgG antibodies was blocked, a remnant of both heavy and light chains were still observed around 50 and 25 kDa (Fig. 7). However, the results showed that mouse IDS was co-immunoprecipitated with specific antibodies against myelin, 14-3-3 proteins zeta (14-3-3Z), 143-3 gamma (14-3-3G), and aldolase C, but did not co-immunoprecipitate with control IgG, Hsp7C, and synaptotagmin (Fig. 7).

IDS-complexes isolation via BN-PAGE. IDS protein-complexes were identified under native conditions, in the cytosolic fractions from brain and in total liver extracts from wild-type mice (Fig. 8A-B). High-molecular mass complexes (HMC) were detected between 232 and 440 kDa and low molecular-mass complexes (LMC) were detected between

Table 2
Proteins purified by affinity chromatography.

Uniprot ID	Name	Mascot score	%SC
Kcrb (Ckb)	Creatine Kinase B-Type	6146.1	44.6
Tba1c	Tubulin Alpha-1c Chain	6125.2	53.9
Atpb	Atpase, Na+/K + Transporting, Beta 1 Polypeptide	5596.4	59.2
Actbl	Beta-Actin-Like Protein 2	4626.4	29.0
At1a3	Sodium/Potassium-Transporting Atpase Subunit Alpha-3	4601.2	48.6
Atpa	Atp Synthase Subunit Alpha, Mitochondrial	4247.6	55.5
Dpyl2	Dihydropyrimidinase-Related Protein 2	4247.1	51.2
Cn37	2′,3′-Cyclic-Nucleotide 3′-Phosphodiesterase	3822.9	49.5
Hsp7c	Heat Shock Cognate 71 Kda Protein	3693.1	45.5
Clh1	Citrate Synthase, Mitochondrial	3506.3	34.1
Stxb1	Syntaxin-Binding Protein 1	3386.7	57.4
Hbb1	Hemoglobin Subunit Beta	3260.2	95.2
Adt1	Adp/Atp Translocase 3	3209.6	50.7
Kpym	Pyruvate Kinase Pkm	3199.5	40.1
At1a2	Sodium/Potassium-Transporting Atpase Subunit Alpha-2	3162.6	33.5
Mdhm	Malate Dehydrogenase, Mitochondrial	3060.6	54.7
At1a1	Sodium/Potassium-Transporting Atpase Subunit Alpha-1	3041.7	32.9
Enog	Tubulin Beta-2a Chain	2844.2	57.6
Aatm	Aspartate Aminotransferase, Mitochondrial	2842.1	40.7
1433z	14-3-3 Protein Zeta/Delta	2635.8	59.2
Aatc	Aspartate Aminotransferase, Cytoplasmic	2524.9	50.6
Enoa	Alpha-Enolase	2366.8	45.4
Vdac1	Voltage-Dependent Anion-Selective Channel Protein 1	2314.6	57.8
Kcc2a	Calcium/Calmodulin-Dependent Protein Kinase Type Ii Subunit Alpha	2236.9	27.6
Gnao	Guanine Nucleotide-Binding Protein G	2217.2	39.8
Acon	Conitate Hydratase, Mitochondrial	2200.0	36.3
G6pi	Glucose-6-Phosphate Isomerase	2157.5	33.9
1433g	14-3-3 Protein Gamma	2124.8	66.8
Nfl	Neurofilament Light Polypeptide	2118.0	34.6
Aldoc	Fructose-Bisphosphate Aldolase C	2088.4	51.5
Mypr (Plp1)	Myelin Proteolipid Protein	2035.6	25.6
Ldhb	L-Lactate Dehydrogenase B Chain	2034.2	48.5
Hs90b	Heat Shock Protein Hsp 90-Beta-Related	1907.6	28.7
Aldoa	Fructose-Bisphosphate Aldolase A	1884.1	50.5
Cmc1	Cox Assembly Mitochondrial Protein Homolog	1851.6	37.7
Gdia	Rab Gdp Dissociation Inhibitor Alpha	1835.5	40.7
Tpis	Triosephosphate Isomerase	1766.2	54.8
Hs90a	Heat Shock Protein Hsp 90-Alpha-Related	1687.8	32.1
Dyn1 (Dnm1)	Dynamin-1	1663.4	32.4
Nsf	Vesicle-Fusing Atpase	1611.4	34.1
Gbb1	Guanine Nucleotide-Binding Protein G	1570.8	41.2
Mdhc	Malate Dehydrogenase, Cytoplasmic	1565.6	40.1
Vata	V-Type Proton Atpase Catalytic Subunit A	1524.2	40.0
Camkv	Cam Kinase-Like Vesicle-Associated Protein	1485.0	28.1
Mbp	Myelin Basic Protein	1447.4	23.2
Arf1	Adp-Ribosylation Factor 1	1388.7	63.0
Ldha	L-Lactate Dehydrogenase A Chain	1325.9	43.1
1433e	14-3-3 Protein Epsilon	1314.4	68.2
Ap2m1	Ap-2 Complex Subunit Mu	1253.7	28.5
1433b	14-3-3 Protein Beta/Alpha	1246.2	58.1
Gabt	4-Aminobutyrate Aminotransferase, Mitochondrial	1226.4	23.2
Hxk1	Hexokinase-1	1165.7	28.9
E41l1	Band 4.1-Like Protein 1	1117.1	13.1
Syt1	Synaptotagmin-1	1115.3	34.4
Kcru	Creatine Kinase U-Type, Mitochondrial	1090.4	22.7
Rab3a	Ras-Related Protein Rab-3a	1064.5	31.4
Ncdn	Neurochondrin	1016.7	32.2
At1b1	Sodium/Potassium-Transporting Atpase Subunit Beta-1	1008.7	29.9
Qcr2	Cytochrome B–C1 Complex Subunit 2, Mitochondrial	1001.6	31.6
Nfm	Neurofilament Medium Polypeptide	992.0	19.5
Stx1b	Syntaxin-1b	979.7	46.9
Gnai2	Guanine Nucleotide-Binding Protein G	971.9	41.1
1433t	14-3-3 Protein Theta	949.5	50.6
Rab10	Ras-Related Protein Rab-10	948.5	35.0
Gdib	Rab Gdp Dissociation Inhibitor Beta	939.1	29.4
Ainx	Alpha-Internexin	925.2	33.5
Ppia	Peptidyl-Prolyl Cis-Trans Isomerase-Related	919.0	50.0
At2b2	Plasma Membrane Calcium-Transporting Atpase 2	894.8	13.4
Snp25	Synaptosomal-Associated Protein 25	893.9	47.6
Odpb	Pyruvate Dehydrogenase E1 Component Subunit Beta, Mitochondrial	869.9	31.8
Cah2	Carbonic Anhydrase 2	864.5	22.3
Pi42b	Phosphatidylinositol 5-Phosphate 4-Kinase Type-2 Beta	863.6	32.0
Cisy	Leukocyte Surface Antigen Cd47	850.1	25.2
1433f	14-3-3 Protein Eta	819.0	43.5
E41l3	Band 4.1-Like Protein 3	812.8	18.3
Pgk1	Phosphoglycerate Kinase 1	795.9	39.1
Sptn1	Spectrin Alpha Chain, Non-Erythrocytic 1	775.1	9.8
Hs71l	Heat Shock 70 Kda Protein 1-Like	773.8	9.5
Idh3a	Isocitrate Dehydrogenase Subunit Alpha, Mitochondrial	770.9	18.3
Odp2	Dihydrolipoyllysine-Residue Acetyltransferase Component Of Pyruvate Dehydrogenase Complex, Mitochondrial	761.4	16.4
Vamp2	Vesicle-Associated Membrane Protein 2	757.8	34.5
Acly	Atp-Citrate Synthase	753.6	6.0
H4	Histone H4	747.1	51.5
Vatb2	V-Type Proton Atpase Subunit B, Brain Isoform	733.0	24.1
At2b1	Plasma Membrane Calcium-Transporting Atpase 1	707.3	12.0
Nfh	Neurofilament Heavy Polypeptide	680.3	15.4
Sodc	Superoxide Dismutase [Cu–Zn]	674.9	32.5
Grp78	78 Kda Glucose-Regulated Protein	666.0	19.8
Eaa2	Excitatory Amino Acid Transporter 2	663.7	15.4
Dpyl3	Dihydropyrimidinase-Related Protein 3	654.8	18.4
Nacam	Nascent Polypeptide-Associated Complex Subunit Alpha, Muscle-Specific Form-Related	654.1	1.8
Dhe3	Glutamate Dehydrogenase 1, Mitochondrial	653.6	25.8
Basp1	Brain Acid Soluble Protein 1	650.1	50.0
Dldh	Dihydrolipoyl Dehydrogenase, Mitochondrial	635.0	25.3
Cof1	Cofilin-1	618.1	44.0
Ndus1	Nadh-Ubiquinone Oxidoreductase 75 Kda Subunit, Mitochondrial	616.7	20.9
Dpyl1	Dihydropyrimidinase-Related Protein 1	607.9	25.0

(*continued on next page*)

Table 2 (*continued*)

Uniprot ID	Name	Mascot score	%SC
Cntn1	Contactin-1	602.3	17.5
Tenr (Tnr)	Adenosine Deaminase Domain-Containing Protein 1	582.0	12.3
Ap1b1	Ap-1 Complex Subunit Beta-1	566.9	15.3
Scot1	Succinyl-Coa:3-Ketoacid Coenzyme A Transferase 1, Mitochondrial	550.6	20.8
Tera	Transitional Endoplasmic Reticulum Atpase	540.7	17.6
Glna	Glutamine Synthetase	536.4	29.2
Sdha	Succinate Dehydrogenase [Ubiquinone] Flavoprotein Subunit, Mitochondrial	532.7	11.4
Park7	Protein Deglycase Dj-1	530.6	14.3
Eaa1	Excitatory Amino Acid Transporter 1	525.8	15.8
Ap2a1	Ap-2 Complex Subunit Alpha-1	515.6	25.1
Ank2	Ankyrin-2	512.0	3.9
Rab2a	Ras-Related Protein Rab-2a	508.2	50.9
A1at1	Alpha-1-Antitrypsin-Related	506.5	15.3
H2a1f	Histone H2a Type 1-B/E	505.9	57.7
Pgam1	Phosphoglycerate Mutase 1	499.2	41.7
Tppp	Tubulin Polymerization-Promoting Protein	469.5	13.3
Hs71a	Heat Shock 70 Kda Protein 1b	443.0	9.5
Sodm	Superoxide Dismutase [Mn], Mitochondrial	424.0	27
Uba1	Ubiquitin-Like Modifier-Activating Enzyme 1	422.0	11.4
Cap1	Prostasin	416.7	15.4
Qcr1	Cytochrome B–C1 Complex Subunit 1, Mitochondrial	409.5	18.3
Sv2b	Synaptic Vesicle Glycoprotein 2b	396.6	12.3
Pdxk	Pyridoxal Kinase	392.1	27.2
Rab6a	Ras-Related Protein Rab-6a	392.0	23.1
Mag	Myelin-Associated Glycoprotein	389.9	6.4
Hba	Hemoglobin Subunit Alpha	362.5	50.7
Ap180	Clathrin Coat Assembly Protein Ap180	351.1	4.1
Gstp1	Glutathione S-Transferase P 1-Related	349.9	26.7
Cand1	Cullin-Associated Nedd8-Dissociated Protein 1	348.1	9.8
Anxa5	Annexin A5	342.3	32.3
Nptn	Neuroplastin	333.1	19.6
Tkt	Discoidin Domain-Containing Receptor 2	332.7	19.1
Cd47	Carbonyl Reductase [Nadph] 1	331.8	4.6
Sptb2	Spectrin Beta Chain, Non-Erythrocytic 1	326.6	6.5
Pura	Transcriptional Activator Protein Pur-Alpha	322.2	15.3
Ndka	Nucleoside Diphosphate Kinase A	320.8	46.1
At1b2	Sodium/Potassium-Transporting Atpase Subunit Beta-2	311.2	24.5
Tmod2	Tropomodulin-2	308.5	10.3
Psb5	Proteasome Subunit Beta Type-5	305.6	29.9
Psa6	Proteasome Subunit Alpha Type-6	304.7	32.1
Ndus3	Nadh Dehydrogenase [Ubiquinone] Iron–Sulfur Protein 3, Mitochondrial	295.2	28.9
Ileua	Leukocyte Elastase Inhibitor	292.2	27.7
Fbx2	F-Box Only Protein 2	290.8	17.2
Prdx2	Peroxiredoxin-2	285.3	33.3
Odo2	Dihydrolipoyllysine-Residue Succinyltransferase Component Of 2-Oxoglutarate Dehydrogenase Complex, Mitochondrial	284.3	7.3
Stx1a	Syntaxin-1a	282.3	23.3
Plpp	Pyridoxal Phosphate Phosphatase	281.7	24.3
Psb3	Proteasome Subunit Beta Type-3	274.4	30.7
Rap1a	Ras-Related Protein Rap-1a	269.9	29.9
Prdx5	Peroxiredoxin-6	269.7	34.3
Prdx6		259.2	47.3
Fril1	Ferritin Light Chain	250.2	26.8
Fscn1	Fascin	247.6	13.8

Table 2 (*continued*)

Uniprot ID	Name	Mascot score	%SC
Otub1	Ubiquitin Thioesterase Otub1	238.4	25.5
Cbr1	Adenylyl Cyclase-Associated Protein 1	234.8	27.1
Vatd	V-Type Proton Atpase Subunit D	234.1	25.1
Roa2	Heterogeneous Nuclear Ribonucleoproteins A2/B1	232.7	13.3
Smd1	Small Nuclear Ribonucleoprotein Sm D1	230.7	24.4
Gna13	Guanine Nucleotide-Binding Protein Subunit Alpha-13	229.4	5.3
Syt5	Synaptotagmin-9	215.0	8.3
Hnrpu	Heterogeneous Nuclear Ribonucleoprotein U	211.9	1.9
Prdx3	Thioredoxin-Dependent Peroxide Reductase, Mitochondrial	211.0	14.4
Arp3b	Actin-Related Protein 3b	208.5	7.7
Rs7	40s Ribosomal Protein S7	202.9	26.3
Pacn1 (Pacsin1)	Protein Kinase C And Casein Kinase Substrate In Neurons Protein 1	201.4	17.9
Hsp74	Heat Shock 70 Kda Protein 4	189.0	8.7
Fumh	Fumarate Hydratase, Mitochondrial	178.4	13.2
Nips1	Protein Nipsnap Homolog 1	177.4	16.5
Crym	Ketimine Reductase Mu-Crystallin	176.8	15.0
Cntp1	Contactin-Associated Protein 1	174.9	6.5
Glsk	Glutaminase Kidney Isoform, Mitochondrial	172.4	9.5
Psb4	Proteasome Subunit Beta Type-4	171.3	11.0
Pp1r7		170.9	11.1
Shps1	Signal-Regulatory Protein Beta-1	168.5	4.9
Rhoa	Transforming Protein Rhoa	167.8	13.0
Gdir1	Rho Gdp-Dissociation Inhibitor 1	167.1	22.1
Ncan	Neurocan Core Protein	163.7	3.2
Psa5	Proteasome Subunit Alpha Type-5	160.0	18.3
Hcd2	3-Hydroxyacyl-Coa Dehydrogenase Type-2	156.4	19.5
Prdx1	Peroxiredoxin-1	154.0	29.1
Negr1	Neuronal Growth Regulator 1	150.4	8.3
Pyc	Pyruvate Carboxylase, Mitochondrial	139.0	6.4
Guad	Guanine Deaminase	133.1	12.3
Pde1b	Calcium/Calmodulin-Dependent 3′,5′-Cyclic Nucleotide Phosphodiesterase 1b	115.9	5.6
Sahh2	Adenosylhomocysteinase 2	115.6	10.8
Lsamp	Limbic System-Associated Membrane Protein	115.1	12.9
Kad1	Adenylate Kinase Isoenzyme 1	108.4	10.3
Nfasc	Neurofascin	107.6	4.4
Neum	Neuromodulin	103.9	18.9
Dopd	D-Dopachrome Decarboxylase	102.1	50.0
Tom70	Mitochondrial Import Receptor Subunit Tom70	92.8	7.2
Wdr1	Wd Repeat-Containing Protein 1	88.7	6.6
Psb6	Proteasome Subunit Beta Type-6	87.6	13.0
Serc	Phosphoserine Aminotransferase	83.7	13.2
Syim	Isoleucine–Trna Ligase, Mitochondrial	83.5	1.5
Dpp3	Dipeptidyl Peptidase 3	77.2	4.3
Nnre	Nad	62.3	10.6
Oat	Ornithine Aminotransferase, Mitochondrial	57.5	6.2
Rpap1	Rna Polymerase Ii-Associated Protein 1	57.2	0.7
Trfe	Serotransferrin	50.7	4.0

66 and 140 kDa (Fig. 8B). Venn and Euler diagrams were constructed to summarize the proteins identified by MS/MS from complexes isolated by BN-PAGE (Fig. 9). Thirteen proteins were identified in the high molecular mass complexes (HMC) mainly composed by hydrolases, oxidoreductases and cytoskeletal proteins, and seventy-two proteins were identified within the low-molecular-mass complexes (LMC) mostly hydrolases, transferases, enzyme modulators, oxidoreductases and

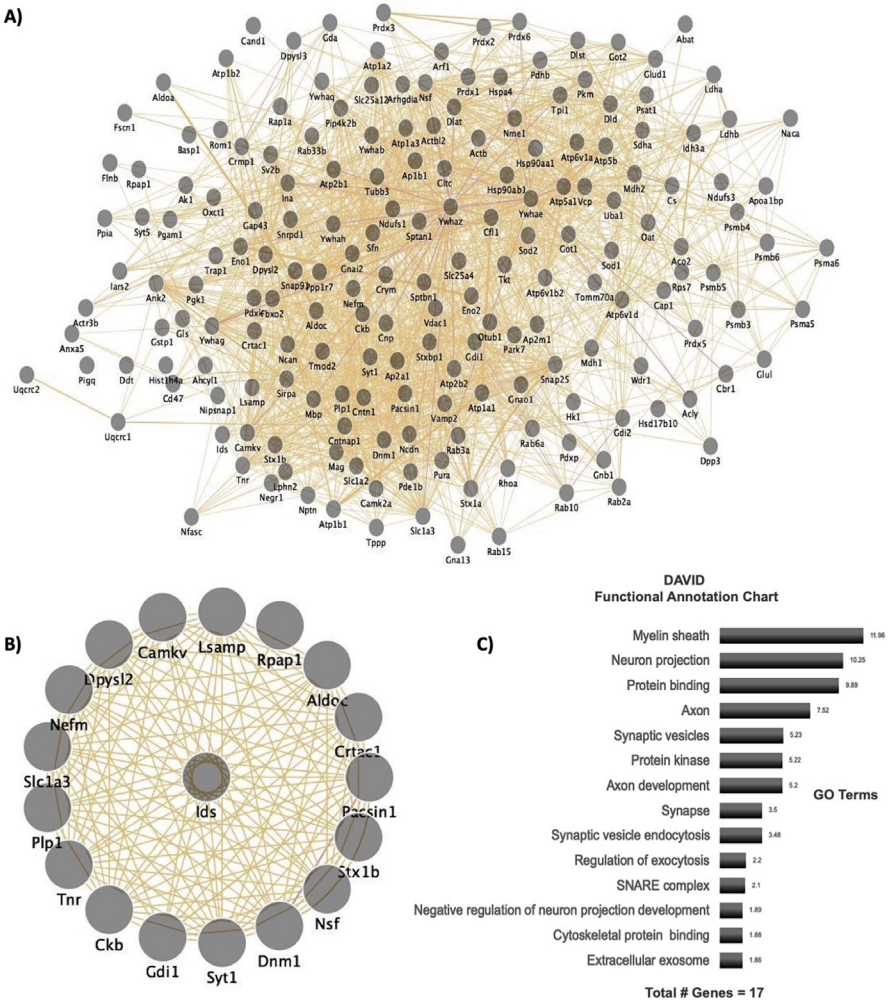

Fig. 5. Bioinformatics analysis of IDS-interacting proteins. A) Interaction map constructed in Cytoscape. GeneMANIA analysis was performed selecting physical and predicted interaction networks and using query gene-based weighting. Known physical interactions were included (purple line) and novel interactions (orange lines) culled from mouse and orthologous protein databases. B) Magnified image of predicted primary IDS-network. C) DAVID GO annotation analysis for the 17 genes included in the primary IDS network.

chaperons, from which only two proteins were found as a common element between these two groups of complexes (Fig. 9).

Bioinformatics analyses of IDS-complexes. To understand the modular properties of the IDS-complexes, bioinformatics analyses were carried out to predict potential clusters and hubs by overlapping complexes via clustering with ClusterONE. This tool allows the detection of groups with high cohesiveness score and growth process from seed-groups to the network expansion. Proteins may have multiple functions

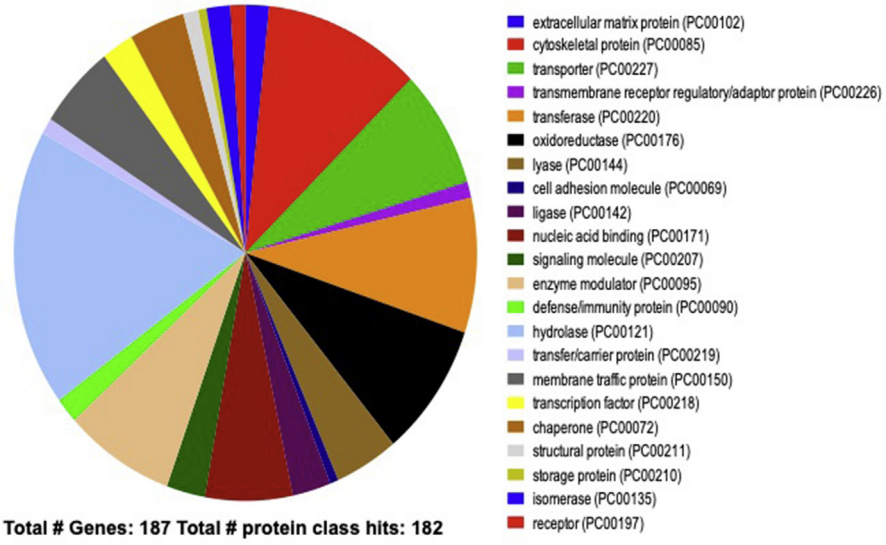

Fig. 6. Protein Analysis Through evolutionary relationships (PANTHER). The proteins were classified according to the molecular function of the protein by itself or with directly interacting proteins at a biochemical level. Chart tooltips are read as: category name (accession): # genes; percent of gene hit against total # genes; percent of gene hit against total # protein class hits.

Table 3
Contextual hub analysis (CHAT) for IDS-proteome.

Hubs	Name	Protein ID	FUNCTION
Ywhaz	14-3-3 protein zeta/delta	P63101	Adapter protein
Ywhaq	14-3-3 protein theta	P68254	Adapter protein
Ywhah	14-3-3 protein eta	P68510	Adaptor Protein
Ywhag	14-3-3 protein gamma	P61982	Adapter protein
Ywhae	14-3-3 protein epsilon	P62259	Adapter protein
Ywhab	14-3-3 protein beta/alpha	Q9CQV8	Adaptor protein
Uba1	ubiquitin-like modifier activating enzyme 1	UBA1	Activates ubiquitin by the adenylating its C-terminal glycine residue with ATP
Sptbn1	Spectrin beta chain, non-erythrocytic 1	SPTB2	Calcium-dependent movement of the cytoskeleton at the membrane
Sptan1	Spectrin alpha chain, non-erythrocytic 1	SPTN1	Interacts with calmodulin in a calcium-dependent manner and is thus candidate for the calcium-dependent movement of the cytoskeleton at the membrane.
Sfn	14-3-3 protein sigma	O70456	Adapter protein
Rab33b	Ras-related protein Rab-33B	RB33B	Protein transport
Rab2a	Ras-related protein Rab-2A	RAB2A	Required for protein transport from the endoplasmic reticulum to the Golgi complex
Prdx2	Peroxiredoxin 2	Q61171	Involved in redox regulation of the cell
Prdx1	Peroxiredoxin-1	PRDX1	Involved in redox regulation of the cell.
Pgam1	Phosphoglycerate mutase 1	Q9DBJ1	Interconversion of 3 and 2-phosphoglycerate with 2,3- bisphosphoglycerate as the primer of the reaction.
Ndufs1	NADH-ubiquinone oxidoreductase 75 kDa subunit, mitochondrial	Q91VD9	Core subunit of the mitochondrial membrane respiratory chain NADH dehydrogenase
Mag	Guanylate-binding protein 1	P20917	Hydrolyzes GTP to GMP in 2 consecutive cleavage reactions
Hspa8	Heat shock protein 8	P63017	Adapter protein implicated in the regulation of a large spectrum of both general and specialized signaling pathways.
Hsp90ab1	Heat shock protein HSP 90-beta	P11499	Molecular chaperone
Hsp90aa1	Heat shock protein HSP 90-alpha	P07901	Molecular chaperone that promotes the maturation, structural maintenance and proper regulation of specific target
Hnrnpu	Heterogeneous nuclear ribonucleoprotein U	Q8VEK3	mRNA processing and stabilization
Gpi1	Glucose-6-phosphate isomerase	P06745	Glycolytic enzyme, function as a tumor-secreted cytokine and an angiogenic factor (AMF) that stimulates endothelial cell motility. GPI is also a neurotrophic factor
Gdi2	Rab GDP dissociation inhibitor beta	Q61598	Regulates the GDP/GTP exchange reaction of most Rab proteins by inhibiting the dissociation of GDP
Fbxo2	F-box only protein 2	Q80UW2	Substrate recognition component of a SCF (SKP1-CUL1-F-box protein) E3 ubiquitin-protein ligase complex
Cltc	Clathrin heavy chain 1	Q68FD5	Clathrin is the major protein of the polyhedral coat of coated pits and vesicles
Cand1	Cullin-associated NEDD8-dissociated protein 1	Q6ZQ38	Ubl conjugation pathway
Camk2a	Calcium/calmodulin-dependent protein kinase type II subunit alpha	P11798	CaM-kinase II (CAMK2) is a prominent kinase in the central nervous system that may function in long-term potentiation and neurotransmitter release
Atp5b	ATP synthase subunit beta, mitochondrial	P56480	Mitochondrial membrane ATP synthase
Ap2m1	AP-2 complex subunit mu	P84091	Component of the adaptor protein complex 2 (AP-2).
Ap2a1	AP-2 complex subunit alpha-1	P17426	Component of the adaptor protein complex 2

and therefore, the corresponding nodes can be part of more than one group of proteins [25]. Biological data sets obtained from IDS-complexes were used to create a corresponding network with geneMANIA and clustered with ClusterONE (Fig. 10A). The identification of contextualized nodes was carried out with CHAT tool (Table 4); while the functional annotation analysis was performed with PANTHER (Fig. 10B). A comparative analysis for HMC and LMC predicted a different topologic architecture (Fig. 10A) due to the differential set of proteins identified in LMC, including transporters, chaperons, enzyme modulators, ligases and immunity proteins. Most of the proteins identified in LMC were carrier proteins and lyases, while oxidoreductases and transcriptional factors were identified in a lower proportion. Conversely, both HMC and LMC have similar content of hydrolases and isomerases proteins (Fig. 10B).

4. Discussion

Protein expression and brain distribution. In humans, IDS is synthesized as a precursor protein, which is matured by trafficking through endoplasmic reticulum, Golgi apparatus, and lysosome, to produce a mature protein with 18 and 42 kDa peptides [33]. Nevertheless, other molecular masses have been reported for wild-type IDS isolated from different sources such as liver, lung, plasma, and urine [34]. Likewise, it is well documented that human IDS overexpressed in mammalian cells showed 72–76 kDa precursors, which are converted into a phosphorylated form of 90 kDa and finally processed to mature forms of 55 and 45 kDa [35,36]. Moreover, human IDS have been expressed in *P. pastoris*, with a molecular mass larger than the one reported for the enzyme produced in mammalian cells [16]. The change in the molecular mass identified in this work could be due to hypermannosylation events, which are commonly observed in proteins expressed in *P. pastoris* [37], and to the fact that IDS sequence contains eight putative N-linked glycosylation sites [38].

Although the histological studies do not include a neuronal cytoplasmic marker for neurons, sagittal brain sections were stained with

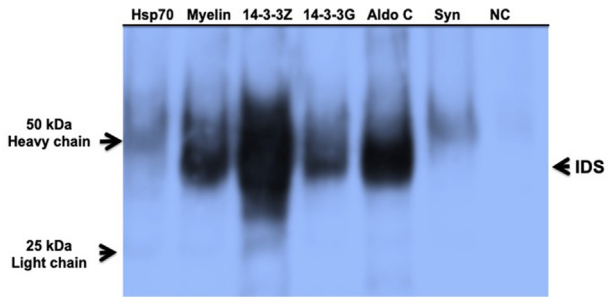

Fig. 7. Co-immunoprecipitation of IDS from mouse brain tissue extracts. Once the proteins are transferred to the nitrocellulose membrane, the light and heavy chains observed as contaminants around 50 and 25 kDa, were blocked with a secondary unconjugated antibody. Immunoblotting was performed using chicken anti-$IDS_{262-286}$. Native IDS was immunopositive for Myelin PLP, 14-3-3 isoform zeta, 14-3-3 isoform gamma and aldolase C. IDS was not detected with anti synaptotagmin (Syn), heat shock protein 70 kDa (Hsp7C) and IgG negative control (NC) (the unedited version is provided in Supplementary Images).

H&E after the immunohistochemistry with specific IDS antibody to determine the cellular distribution of IDS in mouse brain regions. The H&E staining is commonly used as a contrast for the study of cytoplasmic, nuclear, and extracellular matrix features [15]. The IDS staining was observed throughout the layers I-VI from cerebral cortex and the molecular and granular layers of cerebellum, including Purkinge cell layer, suggesting a cytoplasmic reactivity (Fig. 2). In addition, we used the GFAP antibody against a cytoskeletal protein which forms the astrocyte intermediate filaments and has become a regular marker for immunohistochemical identification of astrocytes [39]. The results showed a co-localization of IDS with astrocytes from cortex and cerebellum (Fig. 3).

The widespread IDS distribution in mouse brain was previously reported by Calias *et al.* [40], who showed the distribution of recombinant IDS within the lysosomes of neurons and glial cells in dogs and non-human primates, after the intracerebroventricular and lumbar intrathecal administration of a recombinant IDS. Although the cellular and subcellular location of recombinant IDS has been reported in brain cells of MPS II mice, dogs, and non-human primate models after enzyme replacement therapy [40, 41], the distribution and subcellular localization of this enzyme has not been elucidated under physiological conditions. Notably, recombinant lysosomal enzymes expressed in mammalian cells, like CHO cells, have N-glycans poorly modified with mannose-6-phosphate residues, altering the cell uptake and intracellular trafficking and limiting the use of this data to study wild-type IDS distribution in brain [42, 43]. It has been reported that IDS expression is heterogeneous, with a lower expression in white matter (composed of bundles of myelinated nerve cell projections or axons, connecting various grey matter areas) than in grey matter (cell bodies, glial cells, neuropil and capillaries) [44].

Our results agree to previous immunocytochemical studies, where recombinant IDS was detected in neurons from cerebellar cortex including Purkinge cells and neurons from the surface molecular layer to the deep layer after of treatment [40]. However, this is the first report showing the localization of IDS in nerve cells and astrocytes from cortex and cerebellum under physiological conditions in the mouse brain. Due to the wide brain distribution of IDS, the subsequent proteomics analyses were performed with whole-brain extract instead of an enriched fraction from a particular brain region or a specific cell type.

Bioinformatics analyses of IDS-proteome. The described proteomics approach allowed us to identify 187 IDS-binding proteins mainly classified as hydrolases, cytoskeletal proteins, cell adhesion molecules, oxidoreductases, transferases and transporters. A protein network involved in vesicular transport and neurogenesis was predicted as a primary IDS-network. A similar gene ontology classification was obtained for 41 proteins interacting with human IDS, identified by using

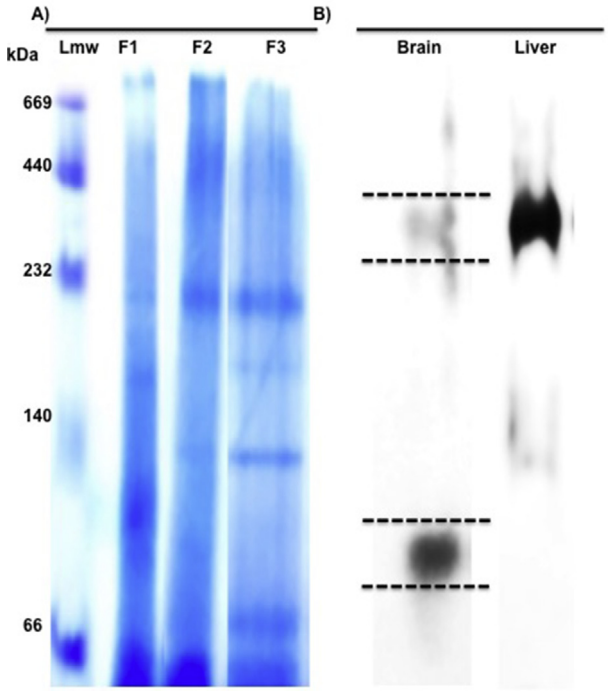

Fig. 8. BN-PAGE and Western blot analysis. A) 60 μg of cytosolic (F1), membranes (F2) and nuclei (F3) protein fractions were subjected to BN-PAGE and stained with Coomassie G-250. B) Western Blot and immunodetection of cytosolic complexes. Proteins from brain and liver were separated and transferred to the nitrocellulose membrane under native conditions, and IDS-complex were immunodetected with specific chicken anti-IDS antibody (1:1000) in an approximate mass of 100 kDa and 300 kD. Segmented lines indicate the bands excised for MS/MS analysis (the unedited versions are provided in Supplementary Images).

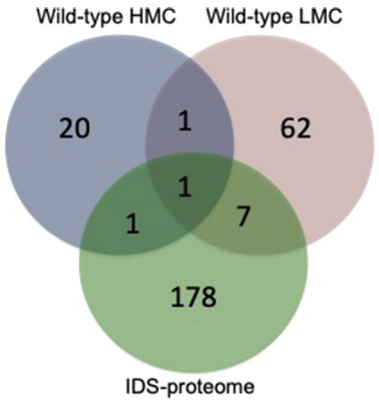

Names	Total	Elements
IDS-proteome Wild-type hmc Wild-type lmc	1	GSTP1_MOUSE
Wild-type hmc Wild-type lmc	1	CE290_MOUSE
IDS-proteome Wild-type hmc	1	PRDX1_MOUSE
IDS-proteome Wild-type lmc	7	PRDX6_MOUSE ENOA_MOUSE PRDX2_MOUSE KCRB_MOUSE ATPA_MOUSE GDIA_MOUSE QCR1_MOUSE

Fig. 9. Venn diagram for native complexes. Venn diagram displays the overlap of proteins identified in each protein complex and the isolated proteome.

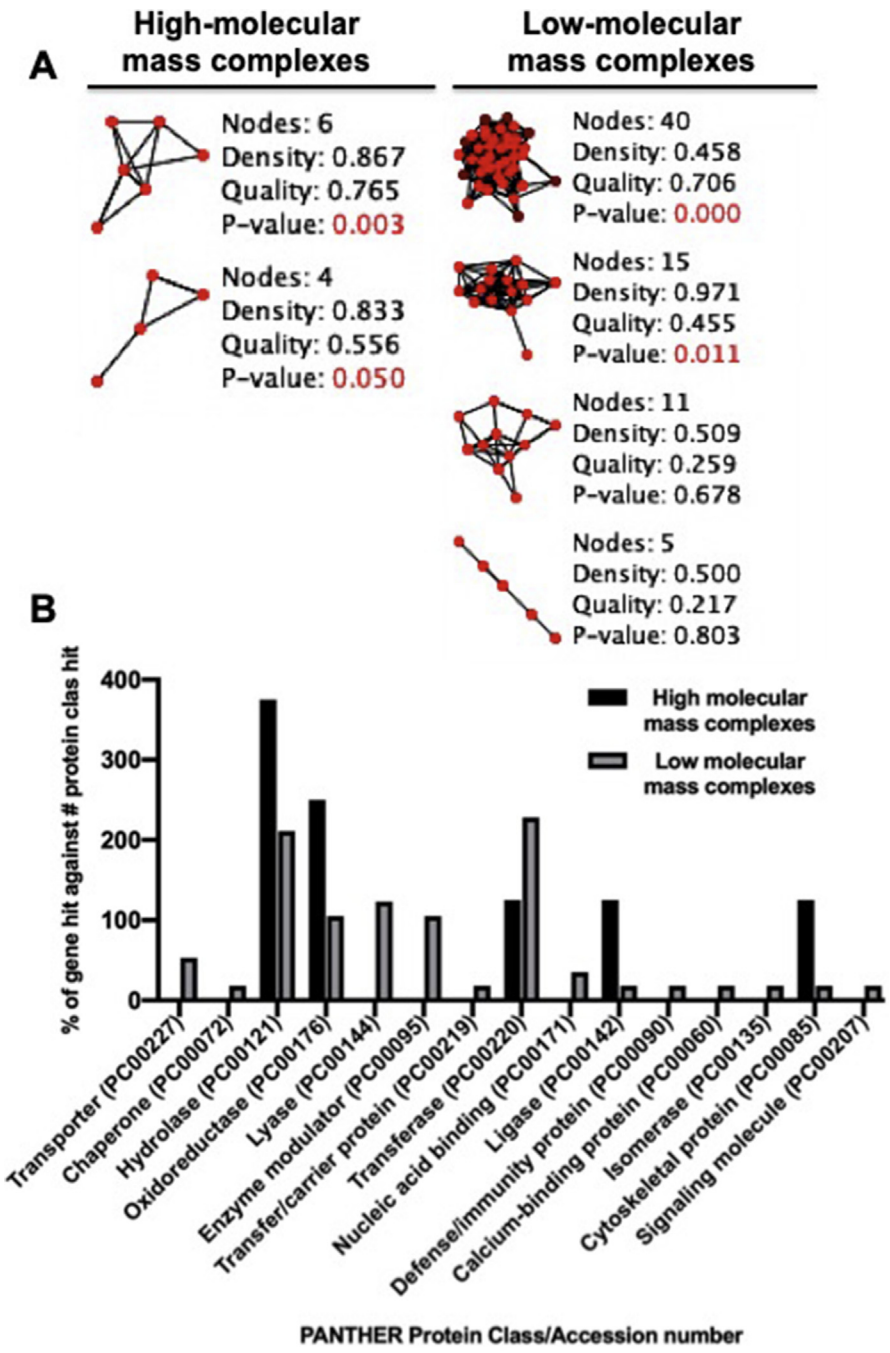

Fig. 10. ClusterONE analyses of high molecular complex for IDS. A) Images corresponding with the selected nodes from a PPI view in Cytoscape. Clusters are ordered according to the p-value. Nodes: number of nodes in the cluster, density: the sum of the edge weights within the cluster divided by the number of theoretically possible edges, quality: ratio (in-weight/(in-weight + out weight), P-value: p-values less than 0.05 are denoted by red colors. B) Functional annotation analysis using PANTHER database. The code corresponding to the protein class (PC) is shown in parentheses.

high-throughput affinity purification and mass spectrometry approaches in HEK293T cells [45]. We performed the affinity purifications in two steps providing advantages over traditional single step methods, such as the reduction of unspecific protein background by using of BSA-columns and increasing high-ionic strength of the binding buffer and washes. To reduce false positives, we used filtering criteria to select the candidates list generated with Mascot, based mainly in reproducibility (proteins must be found in the three independent experiments) [46]. Nevertheless, abundant proteins, such as tubulins that represent the biggest group of cytoskeletal proteins, which were not removed after filtering. These proteins were manually curated and no included in the confirmation study by co-immunoprecipitation. We also found a broad variety of proteins with different molecular functions (Fig. 6) that need to be confirmed as real interactors of IDS.

Moreover, 31 hubs were predicted, which were mainly involved in redox protection (e.g., peroxiredoxins (Prxs) family) and protein transport (e.g., multifunctional *Ywha* genes and different molecular chaperones) (Table 3). These hubs might represent targets for functional analysis, since are topologically and functionally important for biological networks and have been considered as a powerful approach to study biological process in pathological conditions [26, 47].

We confirmed the interaction of four out of the six tested proteins by immunoprecipitation analysis [14-3-3G, 14-3-3Z, Myelin (PLP) and Aldolase C]. Nevertheless, the physiological relevance of these interactions remains unclear. Although the function of 14-3-3 proteins is not completely understood, it is well known that they are abundantly expressed in brain [48], and are crucial for several cellular processes such as cell growth, molecular adhesion signaling and regulation of ion channels [48, 49]. Nevertheless, some mechanisms have been described for these proteins, such as the regulation of enzyme activity of its targets.

Table 4
Identified hubs from high and low molecular mass complexes.

High molecular mass complex			
Gene	Name	Uniprot ID	Function
Prdx1	Peroxiredoxin-1	P35700	Plays a role in cell protection against oxidative stress by detoxifying peroxides and as sensor of hydrogen peroxide-mediated signaling events.
Dync1h1	Cytoplasmic dynein 1 heavy chain 1	Q9JH4	Cytoplasmic dynein 1 acts as a motor for the intracellular retrograde motility of vesicles and organelles along microtubules
Low molecular mass complex			
TXN	Thioredoxin	P10639	Redox reactions through the reversible oxidation of
Prdx2	peroxiredoxin 2	Q61171	Involved in redox regulation of the cell
ATP5B	ATP synthase subunit beta, mitochondrial	P56480	Produces ATP from ADP
ENO1	Alpha-enolase	P17182	Multifunctional enzyme that, as well as its role in glycolysis
Tnip2	TNFAIP3-interacting protein 2	Q99JG7	Inhibits NF-kappa-B activation by blocking the interaction of RIPK1 with its downstream effector NEMO/IKBKG

For example, the interaction between serotonin N-acetyltransferase and 14-3-3Z dimer increases the serotonin activity and the affinity for its substrates, providing an additional protection mechanism for dephosphorylation and/or proteolysis [50, 51]. The control of cellular localization of 14-3-3 proteins binding partners and stimulation of PPI have been documented as well [48]. Notably, human IDS possess a phosphoserine/threonine binding group (pST-bind) at Ser369, while mouse IDS possess two pST-binding sites at Ser156 and Ser14, which are recognition motifs for 14-3-3 proteins (Fig. 11).

We also observed that IDS co-immunoprecipitated with myelin PLP. In the CNS, the oligodendrocytes synthesize the myelin membrane that enwraps the axons to provide the formation and maintenance of the myelin sheath, which is implicated in impulse conduction efficiency [52]. Myelin also contains specific proteins, being the proteolipid protein (PLP) the most abundant one [53]. There is no reported information about the relationship of PLP with any lysosomal protein. However, PLP and lysosomal proteins share some cellular localization sites such as endosomes during intracellular trafficking, since PLP is synthesized in the endoplasmic reticulum, processed through the Golgi apparatus and transported by vesicular transport to the myelin membrane [54]. Alternatively, PLP is also release from late endosomes/lysosomes to the plasma membrane during myelination process [54,55].

Finally, IDS was co-immunoprecpitated with fructose-1,6-(bis) phosphate, aldolase isoform C (Aldo C). Aldo C is the brain specific glycolytic enzyme, which catalyzes the aldol cleavage of fructose-1,6-bisphosphate into glycerinaldehyde-3-phosphate and dihydroxyacetone-phosphate. This protein is expressed mostly in cerebellum, cortex, striatum and hippocampus, but the relevance of this pattern expression is unclear [56, 57, 58].

At present, there are not reports about PPI for IDS. In addition, there are not reports about additional physiological functions of IDS besides its known role in GAGs catabolism. However, the present data suggest that IDS might interact with proteins involved in several cellular processes such as cell growth, molecular adhesion, regulation of enzymatic activity, and intracellular trafficking through the interaction with 14-3-3 zeta and 14-3-3 gamma isoform, biogenesis of myelin through interaction with PLP, and glycolytic pathways through interaction with Aldo C. Nevertheless, the functional purpose of these interactions should be further investigated for a better understanding of these.

Although the global network properties of the brain transcriptome are highly preserved between mouse and human brain, early comparisons indicated that the profiles of orthologous genes differ significantly between each other. Nevertheless, mouse models are still crucial in biomedical research [59]. Although the canonic mouse and human IDS sequences share just an 86% identity, mice models have been used to study MPS II pathophysiology and therapies. For instance, $Ids^{-/-}$ knock out mice have shown that IDS-deficiency generates many of the defects reported for MPS II patients [60]. This fact could suggest that the specific IDS-proteome involved in its processing, transport, function and other roles could be similar.

Analysis of protein complexes. BN-PAGE coupled with nano-HPLC-MS/MS may provide information about the composition of protein complexes and they are commonly used to analyze PPIs and the identification of signal transduction in transient interactions [61, 62]. It has been well accepted that proteins carry out cellular processes through their participation in complexes that play key roles in cell signaling and regulatory process; and they can also bind to DNA and RNA to increase the number of functional possibilities [63]. In this regard, results showed the presence of two IDS-protein complexes in cytosolic fractions and confirmed the presence of 9 proteins also identified by affinity chromatography (Fig. 9). These proteins include Glutathione S-transferase P 1 (GSTP1), Peroxiredoxins (PDRX 2 and 6), Creatine kinases (CKB), Ubiquinol–cytochrome *c* oxidoreductase (QCR1), Rab GDP dissociation inhibitor alpha (GDIA), alfa enolase (ENOA) and ATP synthase subunit alpha, mitochondrial (ATPA).

The protein GSTP1 plays a critical role in cellular detoxification against xenobiotics and noxious compounds as well as against oxidative stress [64]. Peroxiredoxins (PDRX 2 and 6) have an important implication, not only regulating peroxide levels within the cell, but also in oxidative damage protection and the regulation of signalling processes such as growth factor signalling, angiogenesis, toll-like receptor and cytokine signalling [65]. Creatine kinases (CKB), is responsible for the regeneration of ATP and maintenance of energy homeostasis and cytoskeletal dynamics during cell motility [66]. Ubiquinol–cytochrome *c* oxidoreductase (QCR1) is an essential component of the electron transport chain providing chemical energy for cellular metabolism [67]. Rab GDP dissociation inhibitor alpha (GDIA), is a regulator of the Rab small G proteins implicated in neurotransmission based on intracellular vesicle trafficking [68].

We predicted contextualized hubs from wild-type complexes that could be functionally relevant in different biological processes [26] such as dynein and peroxiredoxin-1 (Prdx1) for HMC (Table 4). Cytoplasmic dynein (DnyC1h1) is a microtubule motor protein involved in a wide spectrum of functions including axogenesis, cell migration, macromolecular and vesicular transport [69]. Moreover, dynein drives retrograde axonal transport (movement toward the cell body) and is also involved in lysosome motility [70]. In this sense, recent investigations suggest axonal transport as additional mechanism for intracellular transport of IDS that could be mediated by dynein [69,71].

Interestingly, reactive oxygen species (ROS) induce alterations in brain endothelial protein expression, including proteins involved in cellular redox balances like PDRX1. The overexpression has been

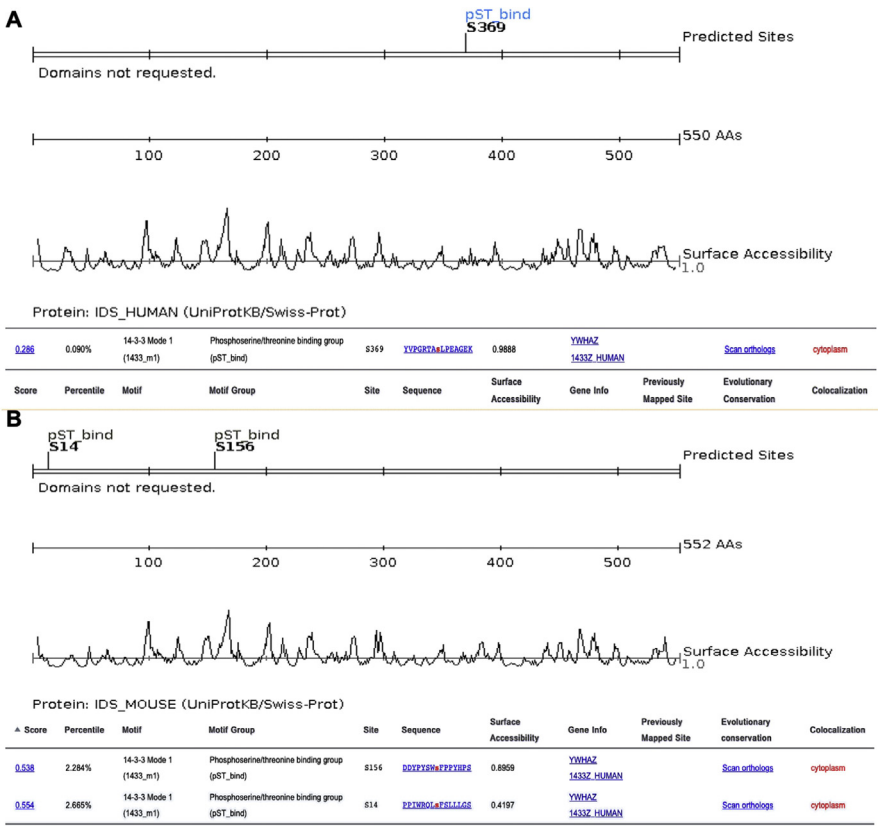

Fig. 11. Motif prediction with Scansite (3 Beta). The figure shows output detailing results for human IDS (A) and mouse IDS (B). A phosphoserine/threonine binding group (pST-bind) was identified at high stringency scoring in human sequence and two binding sites were identified on mouse sequence at low astringency scoring. Motif site, denoted by a vertical line, show an abbreviated name for the identified motif at the corresponding position. The plots of surface accessibility and the amino acid fractional surface probabilities are shown below each cartoon. The default scan condition reveals only motif scoring in the top 0.2858 percentile for human IDS and 2.28 and 2.66 percentile for mouse IDS.

associated with a protection mechanism for brain endothelial cells from ROS-induced damage. PDRX1 also increases brain endothelial monolayer integrity, via a reduction of adhesion molecules expression, which would means that its regulation may be a therapeutic tool to strengthen the blood-brain barrier limiting the cellular infiltration into the CNS and modulate the oxidative stress in neurological diseases [72].

Networks predicted topological attributes of biological relevance with highly interconnected proteins implicated in the same biological processes or specialized functions [25]. However, the topological changes in LMC are probably associated with the increase in the number of proteins with similar or other molecular functions (Fig. 10B). These results are consistent with those obtained through CHAT analysis, due to the identification of different hubs for each group of proteins (Table 4). Five protein hubs were identified for LMC: *i*) TXN1, a small protein involved in cellular redox balance, and associated with neurodegenerative process under oxidative stress conditions [73]; *ii*) TNIP2, which is implicated in the inhibition of nuclear factor-kB(NF-kB) by interacting with TNF-alpha induced protein 3, the activation of signaling pathways during innate immune response, and the regulation of apoptosis in endothelial cells [74, 75]; *iii*) Peroxiredoxin-2 (Prdx2) with antioxidant activity, which it is not only a modulator of intracellular redox signaling but also an activator of Toll-like receptors in inflammation process [76, 77, 78]; *iv*) ATP synthase subunit beta (Atp5b), a mitochondrial membrane enzyme involved in the ATP production from ADP via oxidative phosphorylation (OXPHOS); and *v*) alpha-enolase (ENO1), which is a multifunctional glycolytic enzyme, abundant in cytoplasm, cell surface and nuclei [79]. ENO1 play a key role in cellular stress, autoantigen activities, proliferation and it has also been considered as a tumor marker for diagnosis [80]. Notably, protein families like enolases, peroxiredoxins, tubulins and some cytoskeletal proteins seem to be predominant and frequent in differential proteomics analysis probably due to its abundance [81]. Although the identified complexes are from isolated cytosolic fractions, it is necessary to verify that they are exclusive and not potential contaminant proteins comigratting with IDS. However, important hubs could be promising candidates but the biological relevance in brain should be evaluated experimentally.

In conclusion, our work provides experimental evidences of the localization of IDS in nerve cells and astrocytes from cortex and cerebellum in wild-type mice. In addition, these results show the discovery of binding partners by affinity chromatography and co-immunoprecipitation assays, which have pointed out valuable information toward understanding of how IDS could be implicated in different cellular processes including cell growth, molecular adhesion, regulation of enzymatic activity, intracellular traffic, biogenesis of myelin, and glycolytic pathways. The detection of native cytosolic IDS-complexes and the subsequent modeling of context-specific hubs, allowed the prediction of pathways involved in cell migration, OXPHOS, redox and immune defense, vesicular and axonal transport. In this sense, the origin of the complex Hunter syndrome phenotype might lie in a complex network of IDS interactions that need further studies to understand the significance of these interactions and pathways in Hunter syndrome.

Declarations

Author contribution statement

Carolina Cardona: Conceived and designed the experiments; Performed the experiments; Analyzed and interpreted the data; Wrote the paper.

Carlos J. Alméciga-Díaz: Conceived and designed the experiments; Analyzed and interpreted the data; Wrote the paper.

Luis H. Reyes, Luis Alejandro Barrera: Conceived and designed the experiments; Analyzed and interpreted the data; Wrote the paper.

Eliana Benincore, Natalia Pimentel, Camilo Patarroyo, Alexander Rodríguez-López, M. Martin-Rufian: Analyzed and interpreted the data.

Funding statement

This work was supported by Pontificia Universidad Javeriana and COLCIENCIAS (Grant No. FP44842-233-2015, ID 6699, Análisis de la

expresión de IDS mediante aproximaciones neuroquímicas y proteómicas; and FP44842-232-2015, ID 6700) Alexander Rodríguez-López was supported by Pontificia Universidad Javeriana. Carlos J. Alméciga-Díaz was supported by Pontificia Universidad Javeriana (Grant ID 3964, 5537, and 7204) and COLCIENCIAS (Grant ID 5174, contract No. 120356933205; and Grant ID 5170, contract No. 120356933427).

Competing interest statement

The authors declare no conflict of interest.

Additional information

Supplementary content related to this article has been published online at https://doi.org/10.1016/j.heliyon.2019.e01667

References

[1] E. Neufeld, J. Muenzer, in: D. Valle, et al. (Eds.), The Online Metabolic and Molecular Bases of Inherited Diseases, Vol. III, McGraw-Hill, New York, 2014.
[2] M. Scarpa, in: R.A. Pagon, et al. (Eds.), GeneReviews(R), 1993.
[3] K. Hamano, M. Hayashi, K. Shioda, R. Fukatsu, S. Mizutani, Mechanisms of neurodegeneration in mucopolysaccharidoses II and IIIB: analysis of human brain tissue, Acta Neuropathol. 115 (2008) 547–559.
[4] E.F. Neufeld, Lysosomal storage diseases, Annu. Rev. Biochem. 60 (1991) 257–280.
[5] C.M. Bellettato, M. Scarpa, Pathophysiology of neuropathic lysosomal storage disorders, J. Inherit. Metab. Dis. 33 (2010) 347–362.
[6] J. Muenzer, et al., A phase II/III clinical study of enzyme replacement therapy with idursulfase in mucopolysaccharidosis II (Hunter syndrome), Genet. Med. : Off. J. Am. Coll. Med. Genet. 8 (2006) 465–473.
[7] J. Muenzer, et al., Long-term, open-labeled extension study of idursulfase in the treatment of Hunter syndrome, Genet. Med. : Off. J. Am. Coll. Med. 13 (2011) 95–101.
[8] J. Muenzer, et al., Idursulfase treatment of Hunter syndrome in children younger than 6 years: results from the Hunter Outcome Survey, Genet. Med. : Off. J. Am. Coll. Med. 13 (2011) 102–109.
[9] S.Y. Cho, et al., Effect of systemic high dose enzyme replacement therapy on the improvement of CNS defects in a mouse model of mucopolysaccharidosis type II, Orphanet J. Rare Dis. 10 (2015).
[10] W.M. Caudle, T.K. Bammler, Y. Lin, S. Pan, J. Zhang, Using 'omics' to define pathogenesis and biomarkers of Parkinson's disease, Expert Rev. Neurother. 10 (2010) 925–942.
[11] M.K. Parente, R. Rozen, S.H. Seeholzer, J.H. Wolfe, Integrated analysis of proteome and transcriptome changes in the mucopolysaccharidosis type VII mouse hippocampus, Mol. Genet. Metabol. 118 (1) (2016) 41–54. Epub 2016 Mar 7.
[12] A.C. Sosa, et al., Development of a sandwich enzyme linked immunosorbent assay (ELISA) for the quantification of iduronate-2-sulfate sulfatase, J. Immunol. Methods 368 (2011) 64–70.
[13] U.K. Laemmli, Cleavage of structural proteins during the assembly of the head of bacteriophage T4, Nature 227 (1970) 680–685.
[14] E.D. Morales-Alvarez, et al., Low-scale expression and purification of an active putative iduronate 2-sulfate sulfatase-Like enzyme from Escherichia coli K12, J. Microbiol. 51 (2013) 213–221.
[15] A.H. Fischer, K.A. Jacobson, J. Rose, R. Zeller, Hematoxylin and eosin staining of tissue and cell sections, CSH protoc. 3 (5) (May 2008) pdb prot4986.
[16] N. Pimentel, et al., Production and characterization of a human lysosomal recombinant iduronate-2-sulfatase produced in Pichia pastoris, Biotechnol. Appl. Biochem. 65 (5) (September/October 2018).
[17] M. Urh, D. Simpson, K. Zhao, Affinity chromatography: general methods, Methods Enzymol. 463 (2009) 417–438.
[18] C. von Mering, et al., Comparative assessment of large-scale data sets of protein-protein interactions, Nature 417 (2002) 399–403.
[19] N. Ghosh, G. Sircar, B. Saha, N. Pandey, S.G. Bhattacharya, Data on mass spectrometry based identification of allergens from sunflower (Helianthus annuus L.) pollen proteome, Data Brief 7 (2016) 735–739.
[20] A.G. Woods, et al., ACS Symposium Series, Oxidative Stress: Diagnostics, Prevention, and Therapy, vol. 1083, American Chemical Society, 2011, pp. 341–367. Ch. 12.
[21] I. Wittig, H.-P. Braun, H. Schagger, Blue native PAGE, Nat. Protoc. 1 (2006) 418–428.
[22] G. Dennis Jr., et al., DAVID: database for annotation, visualization, and integrated discovery, Genome Biol. 4 (2003) P3.
[23] H. Mi, et al., The PANTHER database of protein families, subfamilies, functions and pathways, Nucleic Acids Res. 33 (2005) D284–D288.
[24] D. Warde-Farley, et al., The GeneMANIA prediction server: biological network integration for gene prioritization and predicting gene function, Nucleic Acids Res. 38 (2010) W214–W220.
[25] T. Nepusz, H. Yu, A. Paccanaro, Detecting overlapping protein complexes in protein-protein interaction networks, Nat. Methods 9 (2012) 471–472.
[26] T. Muetze, et al., Contextual hub analysis tool (CHAT): a Cytoscape app for identifying contextually relevant hubs in biological networks, F1000Res. 5 (2016) 1745.
[27] E.A.E.A. El-Drieny, et al., Histological and immunohistochemical study of the effect of gold nanoparticles on the brain of adult male albino rat, J. Microsc. Ultrastruct. 3 (2015) 181–190.
[28] A.L. Demain, P. Vaishnav, Production of recombinant proteins by microbes and higher organisms, Biotechnol. Adv. 27 (2009) 297–306.
[29] M. Urh, D. Simpson, K. Zhao, in: R. Burgess Richard, P. Deutscher Murray (Eds.), Methods in Enzymology, vol. 463, Academic Press, 2009, pp. 417–438.
[30] H. Xu, M.A. Freitas, MassMatrix: a database search program for rapid characterization of proteins and peptides from tandem mass spectrometry data, Proteomics 9 (2009) 1548–1555.
[31] C. Shen, et al., On the estimation of false positives in peptide identifications using decoy search strategy, Proteomics 9 (2009) 194–204.
[32] P. Shannon, et al., Cytoscape: a software environment for integrated models of biomolecular interaction networks, Genome Res. 13 (2003) 2498–2504.
[33] A. Daniele, et al., Uptake of recombinant iduronate-2-sulfatase into neuronal and glial cells in vitro, Biochim. Biophys. Acta (BBA) – Mol. Basis Dis. 1588 (2002) 203–209.
[34] J. Bielicki, C. Freeman, P.R. Clements, J.J. Hopwood, Human liver iduronate-2-sulphatase. Purification, characterization and catalytic properties, Biochem. J. 271 (1990) 75–86.
[35] R. Froissart, G. Millat, M. Mathieu, D. Bozon, I. Maire, Processing of iduronate 2-sulphatase in human fibroblasts, Biochem. J. 309 (2) (1995) 425–430.
[36] G. Millat, R. Froissart, I. Maire, D. Bozon, IDS transfer from overexpressing cells to IDS-deficient cells, Exp. Cell Res. 230 (1997) 362–367.
[37] S.H. Teh, M.Y. Fong, Z. Mohamed, Expression and analysis of the glycosylation properties of recombinant human erythropoietin expressed in Pichia pastoris, Genet. Mol. Biol. 34 (2011) 464–470.
[38] M. Demydchuk, et al., Insights into Hunter syndrome from the structure of iduronate-2-sulfatase, Nat. Commun. 8 (2017) 15786.
[39] M.V. Sofroniew, H.V. Vinters, Astrocytes: biology and pathology, Acta Neuropathol. 119 (2010) 7–35.
[40] P. Calias, et al., CNS penetration of intrathecal-lumbar idursulfase in the monkey, dog and mouse: implications for neurological outcomes of lysosomal storage disorder, PLoS One 7 (2012), e30341.
[41] M. Cardone, et al., Correction of Hunter syndrome in the MPSII mouse model by AAV2/8-mediated gene delivery, Hum. Mol. Genet. 15 (2006) 1225–1236.
[42] J.H. Grubb, C. Vogler, W.S. Sly, New strategies for enzyme replacement therapy for lysosomal storage diseases, Rejuvenation Res. 13 (2010) 229–236.
[43] R. Dhami, E.H. Schuchman, Mannose 6-phosphate receptor-mediated uptake is defective in acid sphingomyelinase-deficient macrophages: implications for Niemann-Pick disease enzyme replacement therapy, J. Biol. Chem. 279 (2004) 1526–1532.
[44] E.R. Sowell, P.M. Thompson, K.D. Tessner, A.W. Toga, Mapping continued brain growth and gray matter density reduction in dorsal frontal cortex: inverse relationships during postadolescent brain maturation, J. Neurosci. : Off. J. Soc. Neurosci. 21 (2001) 8819–8829.
[45] Edward L. Huttlin, et al., The BioPlex network: a systematic exploration of the human interactome, Cell 162 (2015) 425–440.
[46] M. Pardo, J.S. Choudhary, Assignment of protein interactions from affinity purification/mass spectrometry data, J. Proteome Res. 11 (3) (2012 Mar 2) 1462–1474. Epub 2012 Feb 10.
[47] A.L. Barabasi, N. Gulbahce, J. Loscalzo, Network medicine: a network-based approach to human disease, Nat. Rev. Genet. 12 (2011) 56–68.
[48] D. Berg, C. Holzmann, O. Riess, 14-3-3 proteins in the nervous system, Nat. Rev. Neurosci. 4 (2003) 752–762.
[49] T. Pawson, J.D. Scott, Signaling through scaffold, anchoring, and adaptor proteins, Science 278 (1997) 2075.
[50] T. Obsil, R. Ghirlando, D.C. Klein, S. Ganguly, F. Dyda, Crystal structure of the 14-3-3zeta:serotonin N-acetyltransferase complex. a role for scaffolding in enzyme regulation, Cell 105 (2001) 257–267.
[51] S. Ganguly, et al., Role of a pineal cAMP-operated arylalkylamine N-acetyltransferase/14-3-3-binding switch in melatonin synthesis, Proc. Natl. Acad. Sci. U.S.A. 98 (2001) 8083–8088.
[52] W. Baron, D. Hoekstra, On the biogenesis of myelin membranes: sorting, trafficking and cell polarity, FEBS Lett. 584 (2010) 1760–1770.
[53] J.M. Boggs, Myelin basic protein: a multifunctional protein, Cell. Mol. Life Sci. : CM 63 (2006) 1945–1961.
[54] W. Baron, et al., The major myelin-resident protein PLP is transported to myelin membranes via a transcytotic mechanism: involvement of sulfatide, Mol. Cell Biol. 35 (2015) 288–302.
[55] A. Feldmann, et al., Transport of the major myelin proteolipid protein is directed by VAMP3 and VAMP7, J. Neurosci. : Off. J. Soc. Neurosci. 31 (2011) 5659–5672.
[56] S. Linke, et al., Aldolase C/zebrin II is released to the extracellular space after stroke and inhibits the network activity of cortical neurons, Neurochem. Res. 31 (2006) 1297–1303.
[57] T.L. Arakaki, et al., Structure of human brain fructose 1,6-(bis)phosphate aldolase: linking isozyme structure with function, Protein Sci. : Publ. Protein Soc. 13 (2004) 3077–3084.
[58] P. Buono, et al., Diverse human aldolase C gene promoter regions are required to direct specific LacZ expression in the hippocampus and Purkinje cells of transgenic mice, FEBS Lett. 578 (2004) 337–344.
[59] R.D. Dowell, The similarity of gene expression between human and mouse tissues, Genome Biol. 12 (2011) 101.

[60] R.S. Holmes, Comparative studies of vertebrate iduronate 2-sulfatase (IDS) genes and proteins: evolution of A mammalian X-linked gene, 3 Biotech 7 (2017) 22.
[61] C.C. Darie, M.L. Biniossek, V. Winter, B. Mutschler, W. Haehnel, Isolation and structural characterization of the Ndh complex from mesophyll and bundle sheath chloroplasts of Zea mays, FEBS J. 272 (2005) 2705–2716.
[62] C.C. Darie, et al., in: Crisan Popescu, Alina D. Zamfir, Nicolae Dinca (Eds.), Applications of Mass Spectrometry in Life Safety, Springer Netherlands, 2008, pp. 3–22.
[63] M.W. Gonzalez, M.G. Kann, Chapter 4: protein interactions and disease, PLoS Comput. Biol. 8 (2012), e1002819.
[64] N. Allocati, M. Masulli, C. Di Ilio, L. Federici, Glutathione transferases: substrates, inihibitors and pro-drugs in cancer and neurodegenerative diseases, Oncogenesis 7 (2018) 8.
[65] A. Perkins, K.J. Nelson, D. Parsonage, L.B. Poole, P.A. Karplus, Peroxiredoxins: guardians against oxidative stress and modulators of peroxide signaling, Trends Biochem. Sci. 40 (2015) 435–445.
[66] J.W. Kuiper, et al., Local ATP generation by brain-type creatine kinase (CK-B) facilitates cell motility, PLoS One 4 (2009), e5030.
[67] P.M. Smith, J.L. Fox, D.R. Winge, Biogenesis of the cytochrome bc(1) complex and role of assembly factors, Biochim. Biophys. Acta 1817 (2012) 276–286.
[68] H. Ishizaki, et al., Role of rab GDP dissociation inhibitor alpha in regulating plasticity of hippocampal neurotransmission, Proc. Natl. Acad. Sci. U.S.A. 97 (2000) 11587–11592.
[69] R.B. Vallee, R.J. McKenney, K.M. Ori-McKenney, Multiple modes of cytoplasmic dynein regulation, Nat. Cell Biol. 14 (2012) 224–230.
[70] E. Chevalier-Larsen, E.L. Holzbaur, Axonal transport and neurodegenerative disease, Biochim. Biophys. Acta 1762 (2006) 1094–1108.
[71] M.A. Passini, E.B. Lee, G.G. Heuer, J.H. Wolfe, Distribution of a lysosomal enzyme in the adult brain by axonal transport and by cells of the rostral migratory stream, J. Neurosci. : Off. J. Soc. Neurosci. 22 (2002) 6437–6446.
[72] G. Schreibelt, et al., Protective effects of peroxiredoxin-1 at the injured blood-brain barrier, Free Radic. Biol. Med. 45 (2008) 256–264.
[73] J. Soerensen, et al., The role of thioredoxin reductases in brain development, PLoS One 3 (2008), e1813.
[74] S. Papoutsopoulou, et al., ABIN-2 is required for optimal activation of Erk MAP kinase in innate immune responses, Nat. Immunol. 7 (2006) 606–615.
[75] S. Van Huffel, F. Delaei, K. Heyninck, D. De Valck, R. Beyaert, Identification of a novel A20-binding inhibitor of nuclear factor-kappa B activation termed ABIN-2, J. Biol. Chem. 276 (2001) 30216–30223.
[76] M.H. Choi, et al., Regulation of PDGF signalling and vascular remodelling by peroxiredoxin II, Nature 435 (2005) 347–353.
[77] T. Shichita, et al., Peroxiredoxin family proteins are key initiators of post-ischemic inflammation in the brain, Nat. Med. 18 (2012) 911–917.
[78] M.C. Sobotta, et al., Peroxiredoxin-2 and STAT3 form a redox relay for H2O2 signaling, Nat. Chem. Biol. 11 (2015) 64–70.
[79] H. Ji, et al., Progress in the biological function of alpha-enolase, Animal Nutrition 2 (2016) 12–17.
[80] P. He, et al., Proteomics-based identification of alpha-enolase as a tumor antigen in non-small lung cancer, Cancer Sci. 98 (2007) 1234–1240.
[81] J. Petrak, et al., Deja vu in proteomics. A hit parade of repeatedly identified differentially expressed proteins, Proteomics 8 (2008) 1744–1749.